

5-2015

## Development of Quantitative Tools for the Characterization and Analysis of the Blood Brain Barrier in Normal and MPS IIIB Mice

Sara M. Rigney  
*Dominican University of California*

<https://doi.org/10.33015/dominican.edu/2015.bio.07>

**Survey: Let us know how this paper benefits you.**

---

### Recommended Citation

Rigney, Sara M., "Development of Quantitative Tools for the Characterization and Analysis of the Blood Brain Barrier in Normal and MPS IIIB Mice" (2015). *Graduate Master's Theses, Capstones, and Culminating Projects*. 187.  
<https://doi.org/10.33015/dominican.edu/2015.bio.07>

This Master's Thesis is brought to you for free and open access by the Student Scholarship at Dominican Scholar. It has been accepted for inclusion in Graduate Master's Theses, Capstones, and Culminating Projects by an authorized administrator of Dominican Scholar. For more information, please contact [michael.pujals@dominican.edu](mailto:michael.pujals@dominican.edu).

**Development of Quantitative Tools for the Characterization and Analysis of the Blood  
Brain Barrier in Normal and MPS IIIB Mice**

A thesis submitted to the faculty of  
Dominican University of California  
& BioMarin Pharmaceutical Inc.

In partial fulfillment of the requirements for the degree

Master of Science  
In  
Biological Sciences

By  
Sara Rigney  
San Rafael, California  
May, 2015

Copyright by  
Sara Rigney  
2015

## CERTIFICATION OF APPROVAL

I certify that I have read *Development of Quantitative Tools for the Characterization and Analysis of the Blood Brain Barrier in Normal and MPS IIIB Mice* by Sara Rigney, and I approved this thesis to be submitted in partial fulfillment of the requirements for the degree: Master of Sciences in Biology at Dominican University of California (and the Buck Institute of Aging or BioMarin Pharmaceutical Inc.).

---

Dr. Anil Bagri MD, PhD  
Graduate Research Advisor

---

Dr. Kiowa Bower PhD  
Second Reader

---

Dr. Maggie Louie PhD  
Graduate Program Coordinator

## Abstract

The Blood Brain Barrier (BBB) functions to control homeostasis within the central nervous system (CNS) via strict control over the passage of molecules into and out of the brain. The goal of this barrier is to protect the CNS from harmful external factors while allowing entry of essential nutrients and removal of metabolic byproducts. This restrictive nature of the BBB is due to the protein network at the borders of adjoining cerebral endothelial cells known as the tight junctions (TJs) and the relationship of other supporting cells and proteins such as astrocytes, pericytes, microglia, and the basement membrane and extracellular matrix proteins associated with the endothelial cells. While beneficial in health, the restrictive nature of the BBB has proved to be a hindrance towards drug administration in many brain diseases, blocking pharmaceutical compounds from diffusing out of the blood vessels and into the brain parenchyma. However, certain diseases such as the metabolic disease Mucopolysaccharidosis IIIB, have been shown to cause breaches in the BBB's integrity, thus suggesting a possible mechanism to administer treatment around this restriction could be to utilize a specific disease's own pathology. In order to understand the extent of BBB dysfunction a systematic and quantitative analysis of the BBB's cellular and protein components and their relationships in each disease of interest during the disease's progression compared to normal conditions is required. This project used advancing technologies in confocal microscopy and 3D image analysis to develop and utilize methodologies to analyze each of the components of the BBB in wild type mice with the goal to quantify their relationship with the cerebral microvascular endothelial cells. In doing so valuable image processing protocols were developed revealing the inadequacies of traditional 2D methods and has helped begin to shed light on the effects of MPS IIIB on the BBB including disrupted endothelial cells along the tight junctions, increased astrocyte contact area and points of contact with endothelial cells, and no changes in the contact area of desmin positive pericytes with endothelial cells.

## Table of Contents

|   |    |
|---|----|
| Introduction .....  | 9  |
| Role of the BBB .....   |    |
| Exclusionary Components of the BBB.....                                 | 9  |
| Endothelial Cells .....   | 9  |
| Tight Junctions .....   | 10 |
| Astrocytes .....  | 10 |
| Pericytes.....  | 11 |
| Extracellular Matrix and Basement Membrane .....                        | 12 |
| Microglia .....   | 12 |
| Challenges of Drug Delivery .....                                       | 12 |
| BBB and Disease .....   | 13 |
| Understanding BBB Breakdown in Metabolic Diseases.....                  | 13 |
| Implications of BBB Disruption .....                                    | 14 |
| Development of Tools to Study the BBB.....                              | 15 |
| Figure 1 The Importance of 3D Analysis.....                             | 18 |
| Materials and Methods.....  | 18 |
| Tissue Preparation .....  | 18 |
| IHC Protocol.....   | 19 |
| Antibody Selection.....   | 19 |
| Table 1: Target Antigens .....  | 19 |
| Phase 1: IHC Protocol Development Antibody Optimization .....           | 20 |
| Table 2: BBB Components Tested Antibodies.....                          | 21 |
| Phase 2: IHC for BBB Characterization .....                             | 21 |
| Table 3: Antibody Staining Combinations.....                            | 22 |
| Image Acquisition.....  | 22 |
| Imaging for Antibody Optimization .....                                 | 22 |
| Imaging for BBB Characterization .....                                  | 23 |
| Image Quantification .....  | 23 |
| Blood Vessel Isolation.....   | 23 |
| Realigning Isolated Blood Vessels.....                                  | 23 |
| Figure 2 Isolation and Realignment of BV in 3D.....                     | 24 |
| Area Measurement of Blood Vessel Cross Sections .....                   | 24 |
| Figure 3: ImageJ Custom Cross Sectional Area Measurement Protocol ..... | 25 |
| Classification of Blood Vessels by Diameter Size .....                  | 26 |
| Astrocyte and Pericyte Surface Area Coverage of Blood Vessels .....     | 26 |

|  |           |
|--|-----------|
| Figure 4: Ex. Of 3D analysis to Measure Pericyte Coverage of Blood Vessels ..... | 27        |
| Astrocyte Points of Contact Measurement .....                                    | 28        |
| Pericyte Volume Measurement .....  | 28        |
| Endothelial Cell Disruption Measurement .....                                    | 28        |
| <b>Results .....</b>   | <b>29</b> |
| <b>IHC Assay Development .....</b>   | <b>29</b> |
| Table 4 Working Antibodies .....   | 30        |
| Endothelial Cell Markers .....   | 30        |
| Figure 5 IHC Assay Development of Endothelial Cell Markers .....                 | 30        |
| Astrocyte Markers .....  | 31        |
| Figure 6 IHC Assay Dev. Of Astrocyte Markers .....                               | 31        |
| Figure 7 GFAP with CD31 Illustrates Astrocyte Interaction with BV .....          | 32        |
| Pericyte Marker .....  | 33        |
| Figure 8 IHC Assay Dev. Of Working Pericyte Markers .....                        | 33        |
| Figure 9 Confocal Image of Desmin and CD31 Costain .....                         | 33        |
| Microglia Marker .....   | 34        |
| Figure 10 IHC Assay Dev of IBA1 .....  | 34        |
| Tight Junction Marker .....  | 34        |
| Figure 11 CD31 Antibodies Function as TJ Marker .....                            | 35        |
| Basement Membrane Markers .....  | 35        |
| <b>Blood Vessel Classification of Average Diameter Calculation .....</b>         | <b>35</b> |
| Table 5 Blood Vessel Diameter Classification .....                               | 36        |
| Table 6 Cortex Blood Vessel Categorization .....                                 | 37        |
| Table 7 Thalamus Blood Vessel Categorization .....                               | 37        |
| <b>Correlation of 2D Vs 3D Vessel Area Measurements .....</b>                    | <b>38</b> |
| Figure 12: No Correlation between 2D and 3D Measurements .....                   | 39        |
| Figure 13: 2D BV Measurements Inaccurate .....                                   | 39        |
| <b>Changes in Astrocyte Foot Process Coverage of MVECs .....</b>                 | <b>40</b> |
| Figure 14 Analysis of Astrocyte and Blood Vessel Interaction Changes .....       | 40        |
| <b>Changes in Astrocyte Foot Process Contact Points .....</b>                    | <b>40</b> |
| Figure 15 Analysis of Astrocyte and Blood Vessel Contact Points .....            | 41        |
| <b>Comparison of Pericyte Coverage of MVECs .....</b>                            | <b>40</b> |
| <b>Analysis of Pericyte Volume .....</b>   | <b>42</b> |
| Figure 16 No Sig. Changes in Surface Area Measurement of Pericytes .....         | 42        |
| Figure 17 Analysis of Pericyte Volume .....                                      | 43        |
| <b>Assessing Endothelial Cell Damage .....</b>                                   | <b>43</b> |

|   |    |
|---|----|
| Figure 18 Comparison of Endothelial Cells .....               | 44 |
| Figure 19 Quantification of Endothelial Cell Disruption ..... | 44 |
| Discussion .....  | 45 |
| Figure 20 Summary of BV Quantification .....                  | 49 |
| Figure 21 Proposed BBB Models .....                           | 53 |
| References .....  | 54 |

**Abbreviations:**

BBB: Blood Brain Barrier

BM: Basement Membrane

CNS: Central Nervous System

Da: Dalton

ERT: Enzyme Replacement Therapy

MVEC: Microvascular Endothelial Cells

MPS: Mucopolysaccharidosis

Naglu: N-acetylglucosaminidase

TJ: Tight Junctions

WT: Wild Type

## **Introduction:**

### ***Role of the Blood Brain Barrier***

The Blood Brain Barrier (BBB) is a physical barricade separating peripheral circulation from the central nervous system (CNS)<sup>1-4</sup>. The primary function of the BBB is to control CNS homeostasis through the selective transport of molecules from the vasculature to the brain and vice versa.<sup>1,2</sup> This selective transport provides the CNS with a specialized protection against harmful external factors while still allowing the influx of essential nutrients<sup>1,2</sup>. Non-specific diffusion across the BBB is restricted to molecules that are lipophilic, contain less than 9 hydrogen bonds, and are less than 400 Da in size<sup>4,5</sup>. All other transport across the barrier is conducted via specific transporters located on the microvascular capillary endothelial cells<sup>5-7</sup>. This strict control is a product of the configuration of several protein networks and cellular components that makeup the BBB<sup>1-5,8</sup>. Below the exclusionary components of the BBB will be discussed in detail.

### ***Exclusionary Components of the Blood Brain Barrier:***

#### ***Endothelial Cells:***

Endothelial cells make up the inner lining of all blood vessels<sup>9</sup>. These cells have the ability to adapt their structure and formation based on their environment and as a result, endothelial cells in the brain possess unique properties compared to their peripheral counterparts<sup>9</sup>. Microvascular endothelial cells (MVECs) are considered the functional location of the BBB due to their lack of pores, that allow quick diffusion through the endothelial cell layer; minimal pinocytosis compared to peripheral endothelial cells; increased mitochondrial activity;

and the presence of tight junctions lining the intercellular border and limiting paracellular diffusion<sup>1-3,10</sup>.

#### *Tight Junctions:*

The tight junctions (TJs) are responsible for restricting the diffusion of water soluble molecules across the MVECs.<sup>1,3,4,11</sup> The TJs are regulated by a complex network of proteins and signaling pathways that include but are not limited to: transmembrane proteins such as junction adhesion molecule-1 (JAM-1), occludin, and claudins; cytoplasmic proteins including zonula occludens 1-3 (ZO1-3); and calcium and phosphorylation pathways<sup>1,4,10,12,13</sup>. While the TJs of the endothelial cells are considered a major component of the BBB, their restrictive nature is not intrinsic but rather an induced property caused by interactions with other protein and cellular components<sup>3,14</sup>. These additional elements of the BBB include astrocytes, pericytes, the extracellular matrix, and basement membrane, are crucial in maintaining and regulating its integrity<sup>1,3,11,15</sup>.

#### *Astrocytes:*

Astrocytes are specialized glial cells that tile the CNS in a non-overlapping, organized manner<sup>16</sup>. In a healthy CNS, astrocytes have roles in development, regulation of blood flow, fluid, ion, pH and transmitter homeostasis, synapse function, CNS metabolism, and form a component of the BBB<sup>16</sup>. When the CNS undergoes trauma, astrocytes respond through a process called reactive astroglyosis, a hallmark of CNS structural lesions<sup>16</sup>. Anatomically, astrocytes have a close association with the cerebral MVECs and are located between the neurons, pericytes and endothelial cells, communicating with these cells through their foot processes<sup>1,3,16</sup>. Functionally, astrocytes are considered to be critical in the development and

maintenance of the BBB; however, the molecular mechanisms and exact roles remain unclear<sup>17,18</sup>. Early studies of astrocytes suggest that their interactions with cerebral MVECs can induce barrier properties in these cells during BBB development, however, other studies have conflicted with this report<sup>1,3,16-20</sup>. Additional studies in mice have demonstrated that the ablation of reactive astrocytes in mice after CNS trauma prevented BBB repair to occur<sup>16</sup>. Alternatively, increased astrocyte number through reactive gliosis alone is not sufficient to restore BBB function<sup>19</sup>. Astrocytes' signaling properties, via calcium pathways, as well as their ability to control blood flow through the secretion of molecular mediators, suggest additional vascular regulatory functions<sup>1,16-18,20</sup>. While most reports vary on the exact role of astrocytes in the BBB, the majority conclude that a more detailed investigation into the role and mechanisms of astrocytes in the BBB are required for a proper understanding of BBB regulation<sup>1-3,16,19-21</sup>. Furthermore, any characterization of the BBB must take the astrocyte component and in particular the glial foot process interaction with endothelial cells into consideration<sup>16,17,21,22</sup>.

#### *Pericytes:*

Pericytes maintain a close association with cerebral MVECs by wrapping around microvascular walls with their finger-like projections, stabilizing vessel formation<sup>23</sup>. Regulatory roles of the pericytes include controlling capillary flow, clearance of cell debris, and regulation of BBB permeability by aiding in restricting endothelial transcytosis<sup>24,25</sup>. Additionally, pericytes have been shown to regulate BBB-specific gene expression as well as induce polarization of the astrocyte endfeet which in turn can induce the barrier like properties in the MVEC.<sup>24</sup> In states of distress, such as hypoxia, pericytes have been observed to migrate away from the brain's MVECs resulting in increased BBB permeability<sup>8</sup>.

### *Extracellular Matrix and Basement Membrane:*

The extracellular matrix (EM) and basement membrane function as an anchor for the MVECs via interactions of laminin and matrix proteins with integrin receptors<sup>2-4</sup>. The basement membrane, is a 30 to 40 nm thick membrane that separates brain endothelial cells from pericytes and astrocytes by ensheathing the capillaries while still bordering the astrocyte foot processes<sup>3</sup>. Protein components of both the EM and basement membrane include collagen, elastin, fibronectin, and laminin, as well as proteoglycans, heparan sulfate, chondroitin sulfate and keratan sulfate. Disruption of the extracellular matrix and/or basement membrane is associated with increased BBB permeability<sup>2-4</sup>.

### *Microglia:*

Microglia are the resident macrophages of the CNS and have been reported by some to potentially play a role in modulating the BBB<sup>1,4,11</sup>. The role of microglia as structural component of the BBB is controversial, however, their ability to regulate vascular permeability via secretion of cytokines suggests that they may have a role in regulating BBB integrity, particularly in the context of states of inflammation<sup>1,4</sup>.

### *Challenges of Drug Delivery into the CNS:*

The blood brain barrier becomes a hindrance toward drug administration in disorders of the CNS<sup>11</sup>. The restriction of large and/or hydrophilic molecules from crossing the BBB cause many therapeutic pharmacological compounds to be excluded from entry into the CNS by the BBB. Most effective treatment methods therefore must often rely on invasive methods, such as intracerebroventricular (ICV) infusions, that bypass the BBB through direct delivery into the CNS<sup>7</sup>. Studies researching the structure and function of the BBB have allowed progress to be

made on finding less invasive methods to target drug delivery to the brain. Strategies that have evolved from these BBB studies include controlling transport receptors to modulate influx of specific drug compounds as well as a more comprehensive approach of increasing BBB permeability<sup>2,5,6,26,27</sup>.

### ***BBB and Disease***

Certain disorders that affect the CNS can cause alterations to the BBB's structure and integrity. The impact of neurodegenerative diseases such as Alzheimer's and Parkinson's diseases' on the BBB have been some of the most extensively studied<sup>4,28</sup>. Other diseases studied include: multiple sclerosis, infectious diseases like meningitis and HIV, epilepsy, stroke, brain tumors and some metabolic diseases<sup>1-3</sup>. In most cases, disease progression is associated with the loss of the BBB's strict transportation control due, in large part, to the disruption of one or more of the cellular components noted above<sup>1-4,21,29,30</sup>

#### *Understanding BBB Breakdown in Metabolic Diseases:*

Little is known about the state of the BBB in most genetic metabolic diseases including the lysosomal storage disorder family, Mucopolysaccharidosis (MPS)<sup>11,27,31</sup>. One member of interest in the MPS family, MPS IIIB also known as Sanfilippo Syndrome, is caused by a deficiency of the enzyme N-acetylglucosaminidase (Naglu)<sup>32</sup>. The lack of Naglu results in the accumulation of heparan sulfate in the lysosomes, causing cerebral and multi-organ abnormalities and ultimately death around the ages of 11-20 years<sup>31</sup>. Currently there is no approved treatment for MPS IIIB however, a common treatment for similar MPS disorders is enzyme replacement therapy (ERT). In order for ERT to be an effective treatment for MPS IIIB it has been hypothesized that the excess heparan sulfate must be cleared from the brain,

therefore, any potential treatment must be able to cross the BBB<sup>27</sup>. Since heparan sulfate accumulation occurs in multiple cell types it is reasonable to hypothesize that there will be changes to BBB structure and function in MPS IIIB. While a few studies to understand the effects this disease has on BBB integrity were done in both humans and in *naglu* knockout mouse models of MPS IIIB the exact nature of these changes remains unclear<sup>31,33-35</sup>. Reported physical changes to the brain in MPS IIIB human patients include cortical atrophy, ventricular enlargement, callosol atrophy, cerebellar changes and purkinje cell abnormalities<sup>35</sup>. One study examined some of the structural impairments of the BBB in MPS IIIB mice and reported leakage of Evans Blue and Albumin, mostly in the cerebellar lobules, cerebral cortex, hippocampus and the midbrain suggesting that MPS IIIB does result in disruption of the BBB but the basis of this disruption is presently unknown<sup>31</sup>. Other findings included degenerating astrocytes, increased number of vascular macrophages, and capillary endothelia abnormalities that increase with age. However, these reports are limited in their analysis and no extensive quantified model of the BBB in MPS IIIB exists yet<sup>31,35</sup>.

#### *Implications of BBB Disruption:*

While the mechanisms may differ amongst disease states, the overall effect of disease on the BBB is altered permeability due to the reorganization and/or loss of TJ proteins, as well as changes in the BBB's supporting cells<sup>2-4</sup>. Although these alterations in permeability can contribute to the physical manifestations of diseases, it also creates the possibility of utilizing these naturally occurring BBB breaches as a pathway for drug administration into the brain<sup>11</sup>. In order to understand the extent of BBB dysfunction and its potential for transport of pharmacologic substances into the brain, a detailed quantitative analysis of the BBB in specific diseases is required.

### ***Development of Tools to Study the BBB***

Protein and cellular components of the BBB can be analyzed in biochemical assays by measuring fluctuations in protein concentrations as well as activity, however, these studies provide no information about the distribution of these components or about their morphological details, such as how many astrocyte foot processes are in contact with a specific blood vessel. *In vitro* models of the BBB have been developed but they cannot perfectly simulate the *in vivo* environment and therefore provide limited information<sup>36,37</sup>. Immunohistochemistry, however, specifically immunofluorescence, offers the ability to visualize and study the localization and morphological details of multiple proteins and cells of interest *in vivo*<sup>38</sup>. Therefore, this technique has the ability to be a powerful tool in characterizing the interactions of the BBB components.

Additionally, advances in microscope and image processing technologies offer new options to increase the capacity of visualization and analysis that were not possible before. Epifluorescence microscopy is the standard form of imaging for most immunofluorescence image analysis<sup>39,40</sup>. In this method, a light source such as a mercury arc lamp is used to excite the fluorophores in the tissue sample. The desired excitation wavelength is set as light from the lamp source passes through an excitation filter placed between the light source and the tissue sample. The excitation light is directed toward the tissue sample by a dichroic mirror. Light that is emitted from the sample's excited fluorophores is then directed upward toward the objective lens and detector. The emitted light passes back through the dichroic mirror and a barrier filter which blocks the shorter wavelengths of the excitation light from reaching the detector<sup>39-41</sup>. The result of this method of microscopy is a 2D image of a single focal plane containing signal only

from the fluorophores excited in the tissue sample. Limitations to this imaging method, however, exist that could make analyzing the BBB interactions of interest in detail difficult. One limitation to epifluorescence microscopy is that the tissue sample is completely illuminated by the excitation light<sup>42</sup>. While most of the light is redirected to the focal point of the detector out of focus light from the surrounding excited tissue area still reaches the detector and creates a haze across the image. In higher objectives and with thicker tissues the amount of out of focus light increases making it difficult to obtain a focused image<sup>39,40,43</sup>. Additionally, epifluorescence microscopes cannot focus through multiple planes limiting the field of view of the images acquired to a single focus plane as well as increasing the amount of out of focus light in the image<sup>39,43,44</sup>.

Confocal microscopy offers a solution to the shortcomings of the epifluorescence microscopy by simply blocking the out of focus light from reaching the detector<sup>39,43,45</sup>. The excitation light source in confocal microscopy is often from a focused laser beam rather than a lamp source limit the surface area of tissue sample that is excited at any specific time. Additionally, a pinhole placed in the emitted light's pathway effectively blocks out of focus light from reaching the detector<sup>39,43</sup>. As a result of this pinhole a further advantage of confocal microscopy is the ability to acquire serial optical sections composed into high resolution image stacks (z-stacks,) which greatly improve the vertical resolution of the image<sup>39,43,44</sup>. These z-stacks can be used to create maximum projections images which provide a better resolved 2D image than can be produced using an epifluorescence. Additionally, these confocal z-stacks can be used to construct 3D reconstructions of the imaged area for a much more detailed image analysis<sup>43,46,47</sup>.

Traditional image processing of histological microscopic images has occurred in 2D utilizing software such as the open access program ImageJ. However, any BBB characterization would require a detailed blood vessel analysis and characterization. An accurate characterization of the blood vessels is necessary as the BBB function, and thus the cellular components interactions, is reported to vary in the different types of microvasculature<sup>45,48,46</sup>. Therefore, before any assertions can be made about how components of the BBB interact with MVECs it is necessary to be able to distinguish between capillaries, venules, and arterioles<sup>48,46</sup>. Typically, histological characterization of blood vessels is performed by measuring the diameter of the blood vessels apparent cross sections in 2D. However, due to the tortuosity of blood vessels and the limited field of view of 2D images traditional methods of measuring 2D vessel diameters can lead to inaccurate characterization of vessels by measuring regions that are too long, short or not the true diameter<sup>46,49</sup>. (Fig.1). This limitation of 2D measurement is hypothesized to be a factor in the variability of characterization parameters of the BBB which are proposed to be highly sensitive to vessel diameter<sup>46</sup>. The development and improvement of 3D software offers a possible solution to the short comings of 2D analysis and should be a valuable asset in developing both WT and MPS IIIB BBB models<sup>47,50</sup>. The BBB with its many interacting components offers a great model system to explore the advantages of 3D analysis over 2D.

In order to have an in depth understanding of the changes that occur in the BBB during disease the structural components of the BBB must be able to be characterized in a reliable and reproducible manner. This study aims to utilize the specificity of immunohistochemistry assays and advancements in 3D image processing to develop a unique quantitative structural model of the protein and cellular components of the BBB in both wild type and MPS III mouse models. The overall goal in creating this model is to find a reliable and reproducible method of

characterizing the BBB in both normal and diseased animals in order to provide useful information on the pathophysiology and to help in identifying the best methods for therapeutic intervention.

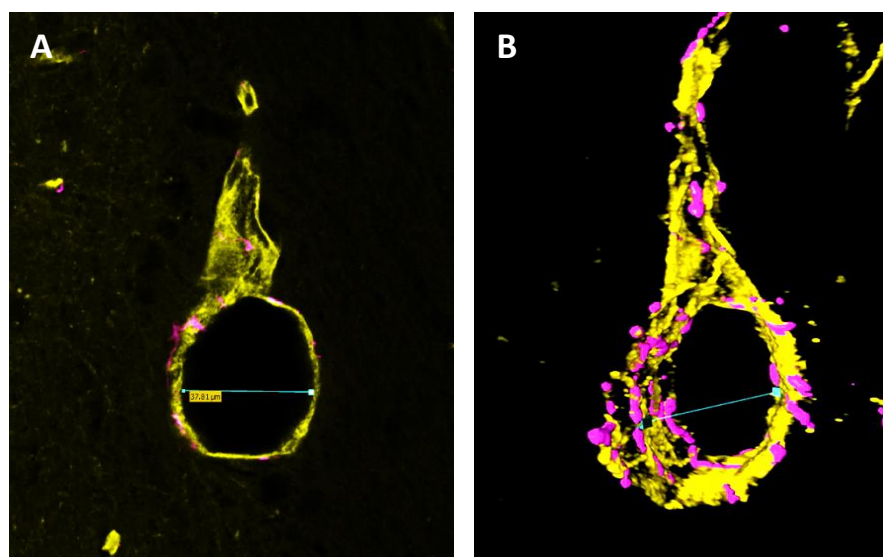


**Figure 1: The Importance of 3D Analysis in Blood Vessel Characterization in BBB Analysis**

A) The 2D measurement of what appears to be a blood vessels cross section B) 3D rendering of the same blood vessel and line measurement shows the line drawn is not across the diameter but rather at a diagonal from one end of the blood vessel to the other. 3D measurement may provide a more accurate method of measuring and

## Materials and Methods:

### Tissue Preparation

Tissues were perfusion fixed with formalin to preserve vascular structure and then cryoprotected with 30% sucrose solution to reduce artifacts that are commonly introduced during tissue freezing. Frozen tissues were sectioned on a cryostat into 50  $\mu\text{m}$  thick sections. For short term storage tissues were stored in 1X PBS solution with 0.01%  $\text{NaN}_3$  at 4°C. For long term storage tissues were stored at -20°C in a cryoprotectant buffer of 30% sucrose (w/v), 1% polyvinyl-pyrrolidone (w/v), 50 % 0.1M phosphate buffer (v/v), and 30% ethylene glycol (v/v).

### IHC Protocol

#### *Antibody Selection:*

Antibodies to detect astrocytes, pericytes, microglia, tight junctions, and the basement membrane/extracellular matrix were tested and optimized through a series of IHC experiments. A description of the target antigens to label each BBB component can be seen in Table 1 and the full list of tested antibodies can be viewed in Table 2. A secondary antibody for mouse IgG was also used alone to detect endogenous IgG in order to measure vascular leakage across the BBB.

**Table 1: Target Antigens for Labeling Blood Brain Barrier Components**

| <b>BBB Component</b>     | <b>Antigen</b>         | <b>Description</b>  |
|--------------------------|------------------------|---|
| <b>Endothelial Cells</b> | CD31                   | <ul style="list-style-type: none"> <li>• Also known as Platelet Endothelial Cell Adhesion Molecule (PECAM-1).</li> <li>• Integral membrane glycoprotein expressed on platelets, monocytes, neutrophils, some T cells, and concentrated at endothelial cell borders</li> </ul> |
| <b>Tight Junctions</b>   | ZO-1                   | <ul style="list-style-type: none"> <li>• Zonula occluden 1</li> <li>• Peripheral membrane protein of the tight junctions</li> <li>• Expressed on the cytoplasmic surface of endothelial cells</li> </ul>  |
|                          | Occludin               | <ul style="list-style-type: none"> <li>• Integral plasma membrane tight junction protein</li> <li>• Main component of the tight junctions</li> </ul>  |
|                          | E-Cadherin             | <ul style="list-style-type: none"> <li>• Endothelial cell specific adhesion molecule</li> <li>• Located at junctions between endothelial cells</li> </ul>   |
|                          | Claudin-1<br>Claudin-5 | <ul style="list-style-type: none"> <li>• Members of the Claudin trans membrane tight junction protein family</li> </ul>   |
| <b>Astrocytes</b>        | GFAP                   | <ul style="list-style-type: none"> <li>• Glial Fibrillary Acid Protein</li> <li>• Class III intermediate filament protein expressed in astrocytes</li> <li>• Distinguishes astrocytes from other glial cells during development</li> </ul>                                    |
| <b>Pericytes</b>         | PDGFRB                 | <ul style="list-style-type: none"> <li>• Tyrosine-kinase receptor</li> <li>• Expressed by pericytes, fibroblasts and astrocytes</li> </ul>  |
|                          | ASMA                   | <ul style="list-style-type: none"> <li>• Alpha Smooth Muscle Actin</li> <li>• Expressed in the internal structure of smooth muscle cells and pericytes</li> </ul>   |
|                          | NG2                    | <ul style="list-style-type: none"> <li>• Neuronglial 2</li> <li>• Membrane chondroitin sulfate protein</li> <li>• Expressed on surface of pericytes, glial precursor cells, chondroblasts and proliferating capillary endothelial cells</li> </ul>                            |
|                          | Desmin                 | <ul style="list-style-type: none"> <li>• Muscle specific class III Intermediate Filament protein</li> <li>• Expressed on most muscle types and pericytes</li> </ul>   |
| <b>Basement Membrane</b> | Collagen IV            | <ul style="list-style-type: none"> <li>• Major structural component of basement membranes</li> </ul>  |
| <b>Microglia</b>         | IBA1                   | <ul style="list-style-type: none"> <li>• Ionizing Calcium-Binding Adaptor Molecule 1</li> <li>• Specifically expressed in macrophages and microglia</li> <li>• Up regulated expression during microglia activation</li> </ul>   |

### ***Phase 1 Development: IHC Protocol Development Antibody Optimization***

Sections were stained while floating in 6 and 12 well plates rather than mounted on a slide in order to improve antibody penetration and staining quality. An immunohistochemistry staining protocol was developed to accommodate these thick floating tissue sections. In a twelve well plate, sections were first washed in PBS plus 0.3% Triton-X (PBT) for 15 minutes followed by incubation in 10% blocking serum (animal host of the secondary antibody) for one hour. After blocking sections were incubated in primary antibody diluted in 2% normal serum overnight at 4°C. Primary antibody concentrations varied based on the antibody and were determined for each candidate through a series of optimization experiments to determine the dilution that produced the best signal to noise ratio before they could be used in this analysis. Controls for each IHC experiment were placed in a well containing incubation buffer without antibody. Following primary incubations tissues were washed as follows: 3 x 20 min; 3x 1 hour for a total of four hours in 6 well plates. Tissue samples were then transferred to 12 well plates and incubated in secondary antibody diluted in 2% normal serum for one hour at room temperature. Secondary antibody concentrations were optimized for each primary. Following secondary antibody incubations samples were washed in PBT following the same four hour wash that occurred after primary incubation. The sections were then counterstained with DAPI (0.1 µg/mL, 5 min), washed (3x15 min), mounted on slides, and cover-slipped with Fluoromount (Sigma/F4680-25ML).

**Table 2: BBB Components Tested Antibodies**

| <b>Marker</b>            | <b>Antibody</b>     | <b>Supplier/Catalog Number</b> | <b>Host Species</b> | <b>Concentration</b> |
|--------------------------|---------------------|--------------------------------|---------------------|----------------------|
| <b>Endothelial Cells</b> | <b>CD31</b>         | RD Systems/AF3628              | Goat                | 0.2 mg/mL            |
|                          | <b>CD31</b>         | Abcam/ab28364                  | Rabbit              | Not Specified        |
|                          | <b>CD31</b>         | Sigma/SAB4502167               | Rabbit              | 1mg/mL               |
|                          | <b>CD31</b>         | Millipore/CBL1337              | Rat                 | 0.5 mg/mL            |
|                          | <b>CD31</b>         | Abcam/ab56299                  | Rat                 | 0.5 mg/mL            |
|                          | <b>Isolectin B4</b> | Life Technologies/I21411       | N/A                 | 1 mg/mL              |
| <b>Astrocytes</b>        | <b>GFAP</b>         | Sigma/SAB2500462               | Goat                | 0.5mg/mL             |
|                          | <b>GFAP</b>         | Sigma/ G3893                   | Mouse               | Not Specified        |
|                          | <b>GFAP</b>         | Invitrogen/13-0300             | Rat                 | 0.5 mg/mL            |
| <b>Pericytes</b>         | <b>Desmin</b>       | Novus/NB120-15200              | Rabbit              | 0.2 mg/mL            |
|                          | <b>PDGFRB</b>       | Novus/NBP1-43349               | Rat                 | 0.5 mg/mL            |
|                          | <b>ASMA</b>         | Novus/NB110-55432              | Rabbit              | Not Specified        |
|                          | <b>PDGRB</b>        | Cell Signaling/3169            | Rabbit              | Not Specified        |
|                          | <b>NG2</b>          | Millipore/MAB5384              | Mouse               | 1 mg/mL              |
|                          | <b>NG2</b>          | Millipore/AB5320               | Rabbit              | 1 mg/mL              |
|                          | <b>ASMA</b>         | Abcam/ab7817                   | Mouse               | 0.2 mg/mL            |
|                          | <b>ASMA</b>         | Abcam/ab5694                   | Rabbit              | 0.2 mg/mL            |
| <b>Microglia</b>         | <b>IBA1</b>         | Abcam/AB5076                   | Goat                | Not Specified        |
| <b>Basement Membrane</b> | <b>Collagen IV</b>  | Millipore/AB769                | Goat                | 0.4 mg/mL            |
|                          | <b>Collagen IV</b>  | Abcam/ab19808                  | Rabbit              | Not Specified        |
| <b>Tight Junctions</b>   | <b>ZO-1</b>         | Invitrogen/33-9100             | Mouse               | 0.5 mg/mL            |
|                          | <b>ZO-1</b>         | Invitrogen/61-7300             | Rabbit              | 0.25 mg/mL           |
|                          | <b>Occludin</b>     | Invitrogen/33-1500             | Mouse               | 0.5 mg/mL            |
|                          | <b>Occludin</b>     | Invitrogen/71-1500             | Rabbit              | 0.25 mg/mL           |
|                          | <b>E-Cadherin</b>   | Invitrogen/33-4000             | Mouse               | 0.5 mg/mL            |
|                          | <b>Claudin-1</b>    | Invitrogen/51-9000             | Rabbit              | 0.25 mg/mL           |
|                          | <b>Claudin-1</b>    | Invitrogen/37-4900             | Mouse               | 0.5 mg/mL            |
|                          | <b>Claudin-5</b>    | Invitrogen/35-2500             | Mouse               | 0.5 mg/mL            |

**Phase 2: IHC for BBB Characterization**

Using the IHC protocol and tested antibodies from phase one both WT and MPS IIIB brain tissue sections from -1.28 to -2.75 mm of bregma were stained in the combinations listed in Table 3.

**Table 3: Antibody Staining Combinations for BBB Characterization**

| <b>BBB Components</b>   | <b>Primary Antibodies</b> | <b>Secondary Antibodies</b>                            | <b>Blocking Serum</b>                      |
|---|---------------------------|--|--|
| <b>Endothelial Cells</b><br><b>Astrocytes</b><br><b>Pericytes</b> | Goat anti CD31            | Donkey anti Goat Alexa Fluor 555 (Life Technologies)   | Normal Donkey Serum (Jackson Laboratories) |
|   | Rat anti GFAP             | Donkey anti Rat Alexa Fluor 647 (Abcam Inc.)           |  |
|   | Rabbit anti Desmin        | Donkey anti Rabbit Alexa Fluor 488 (Life Technologies) |  |
| <b>Endothelial Cells</b><br><b>Basement Membrane</b>              | Rabbit anti CD31          | Donkey anti Rabbit Alexa Fluor 555 (Life Technologies) | Normal Donkey Serum (Jackson Laboratories) |
|   | Goat anti Collagen IV     | Donkey anti Goat Alexa Fluor 488 (Life Technologies)   |  |
| <b>Endothelial Cells</b><br><b>Microglia</b>                      | Rabbit anti CD31          | Donkey anti Rabbit Alexa Fluor 555 (Life Technologies) | Normal Donkey Serum (Jackson Laboratories) |
|   | Goat anti IBA1            | Donkey anti Goat Alexa Fluor 488 (Life Technologies)   |  |
|   | Goat anti CD31            | Donkey anti Goat Alexa Fluor 555 (Life Technologies)   |  |
| <b>Endothelial Cells</b><br><b>IgG</b>                            | Goat anti CD31            | Donkey anti Goat Alexa Fluor 555 (Life Technologies)   | Normal Donkey Serum (Jackson Laboratories) |
|   | Donkey anti Mouse 488     | N/A  |  |

**Image Acquisition:****Phase One: Imaging for Antibody Optimization**

Initial image analysis of the antibody testing experiments used a Leica DM 4000 series fluorescence microscope at 20x and 40x oil objectives.

**Phase Two: Imaging for BBB Characterization:**

Due to the use of thick tissue sections and the limitations described earlier of the epifluorescence microscope, particularly out of focus light effecting the image quality and the inability to image more than one focal plane, a confocal microscope was required to produce image stacks (z-stacks) at both a high objective and resolution. Images used in quantification protocol development and BBB characterization were acquired using a Leica TCS SP8 confocal

microscope. Images were acquired at a 40x objective with the number of z-stack slices varying in order to capture the maximized depth in the z-axis. Image files acquired from the Leica TCS SP8 confocal microscope were saved and exported as lif files.

### **Image Quantification:**

#### ***Blood Vessel Isolation:***

Using the commercially available Volocity, a 3D image visualization and quantification software program by Perkin Elmer, 3D representations were constructed from the blood vessel z-stacks acquired from confocal microscopy (Fig. 2A). The confocal lif image stack files were imported into Volocity. Blood vessels of interest were isolated using a measurement protocol developed in Volocity's quantification program. Blood vessel populations were created through a threshold detected and filtered by volume size ( $\mu\text{m}^3$ ) starting at  $5000 \mu\text{m}^3$  and adjusted until just the vessel of interest was selected. A region of interest (ROI) was then created of the selected blood vessel of interest (Fig. 2B). The image was then cropped to the selection and a new 3D image was automatically generated containing just the vessel of interest (Fig. 2C).

#### ***Realigning Isolated Blood Vessels:***

Isolated blood vessels were resliced to align the vessel cross section along the xy axis. An ROI of the blood vessel was again created by a threshold detection. When the vessel image with the ROI is viewed in Volocity's 3D slice mode a 3D isosurface representation of the blood vessels was created from the ROI (Fig. 2D). The 3D vessel representation was then rotated around its axis until the vessel cross section was aligned along the image's xy plane (Fig. 2E). The image was then resliced and a new image created with the desired vessel orientation (Fig. 2F).

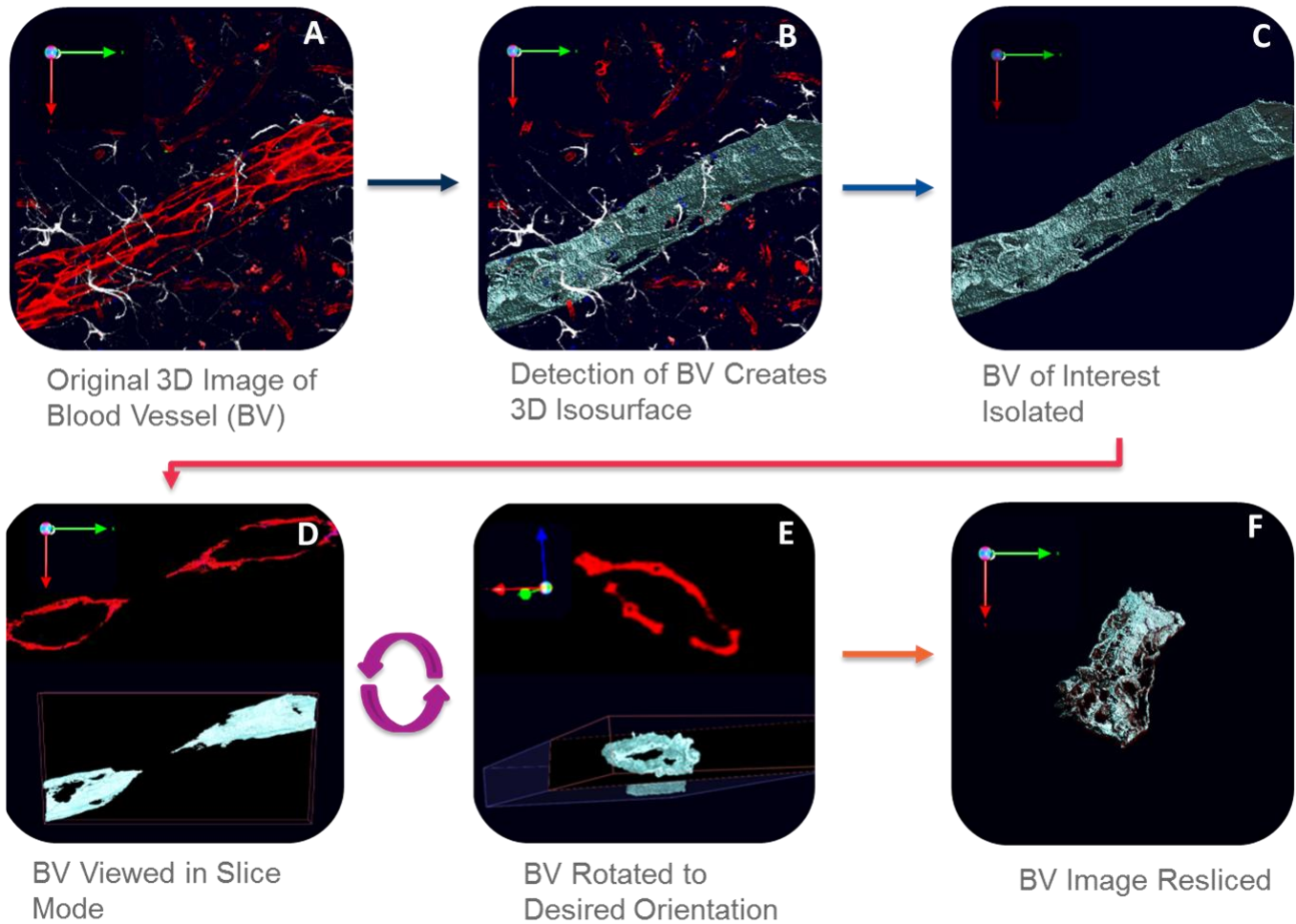


**Figure 2: Isolation and Realignment of Blood Vessels in 3D** Using 3D reconstructions of the blood vessel image stacks (A), taken with a confocal microscope, the blood vessels can be threshold detected to create an isosurface region of interest (B); isolated from the rest of the image (C) and realigned so that their cross sections and therefore their diameters align with the xy plane, so that you are looking down the true cross section of the vessel, then we virtually re-sectioned the vessel (D-F).

### *Area Measurement of Blood Vessel Cross Sections:*

The resliced blood vessel image stacks were exported from Volocity as ics/ids files in order to be imported into ImageJ. In ImageJ the ics/ids vessel image stack files were split into individual channel image stacks. The CD31 channel, representing endothelial cells, image stacks were saved as tiff files. These CD31 tiff images were batch processed to measure the interior area of the blood vessel cross section of each slice in the image stack using a custom measurement macro (Fig. 2). The results table generated were saved and exported into Microsoft

Excel where data for each vessel image were sorted by file name. The diameters for each measured slice were calculated from the area. All slice diameters were averaged to determine the average cross section diameter for each blood vessel. As a control, a 3D cylinder volume was created from a stack of 2D circles drawn with a known diameter and micron/pixel scale. This control image stack was imported into Volocity where the 3D volume was constructed and underwent the same detection, isolating, and reslicing as the blood vessel volumes. The control volume image stack was then exported from Volocity as an ics/ids file and imported into ImageJ where it underwent the same cross sectional area measurements as each of the blood vessel image stacks.

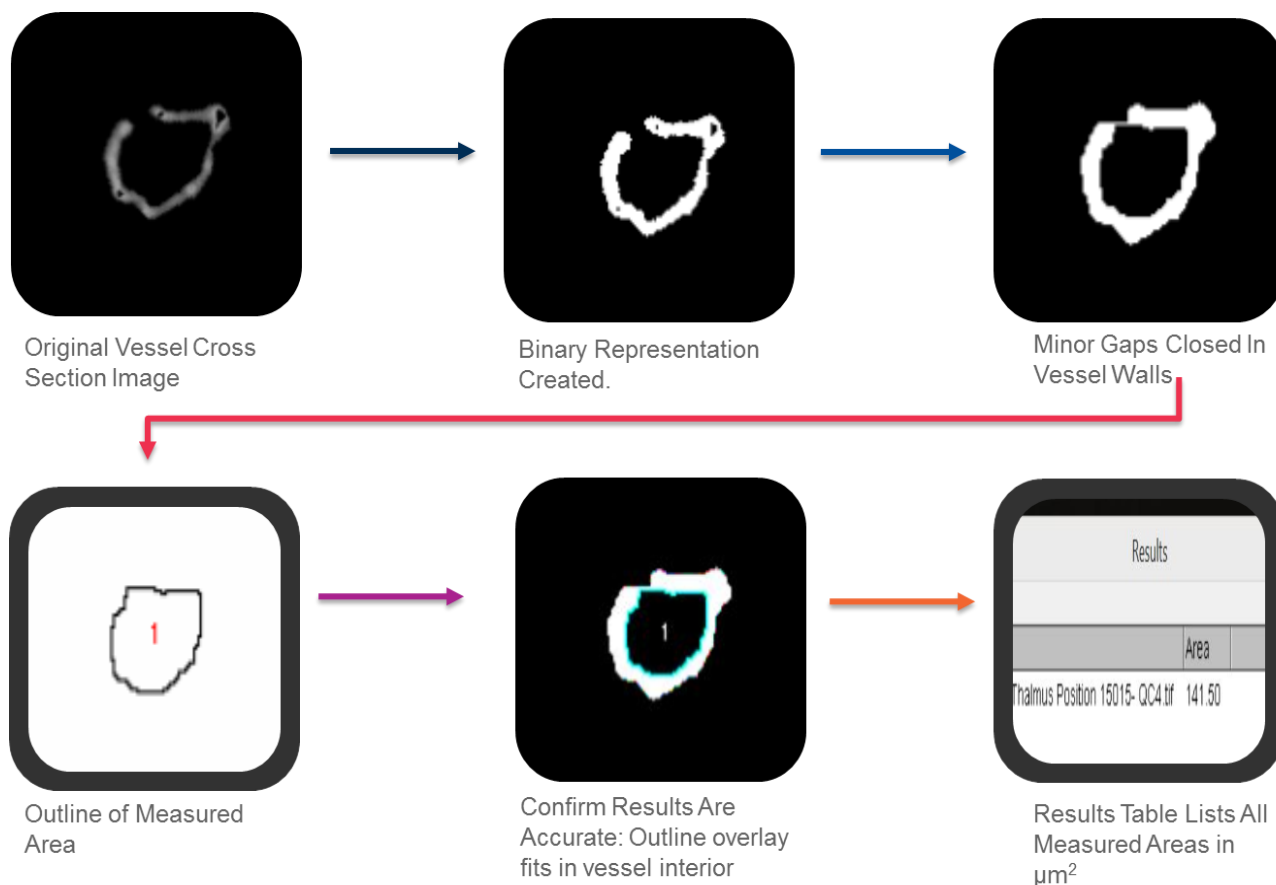


**Figure 3: ImageJ Custom Cross Sectional Area Measurement Protocol:** For each slice in a stack the threshold detection was set to 1-255. A binary representation of each image slice was created and inverted. An open command was run to fill any minor gaps in vessel walls. Measurements run were for object area. Size limitations of 25-500  $\mu\text{m}^2$  was set to eliminate noise detection. Outline images of what was measured in each slice were created. Results were displayed in a results table later exported into Microsoft Excel.

***Classification of Blood Vessels by Diameter Size:***

The average cross section diameters were used to classify each of the measured blood vessels into three categories: capillaries:  $< 10 \mu\text{m}$ , pre and post capillary arterioles and venules:  $11\text{-}20 \mu\text{m}$ , and arterioles and venules:  $> 20 \mu\text{m}$ . Image files of vessels in the capillary and pre and post capillary vessel groups were used in further quantitative analysis for BBB characterization. Vessels in these two groups represent the largest components of the vascular surface area within the brain and the vessels where BBB is most critical.

***Astrocyte and Pericyte Surface Area Coverage of Blood Vessels:***

Blood vessel, astrocyte and pericyte populations were created through threshold detection of each respected channel. Two new populations called Astrocyte Intersection and Pericyte Intersection were created to detect where voxels (3D pixels) from each astrocyte or pericyte channel coexisted with the blood vessel channel by using the “intersect” command in Volocity. (Fig. 4). Surface area measurements ( $\mu\text{m}^2$ ) of the astrocyte intersection and pericyte intersection populations were performed simultaneously. The measurement results were exported into Microsoft Excel for further analysis of astrocyte and pericyte coverage of blood vessels.

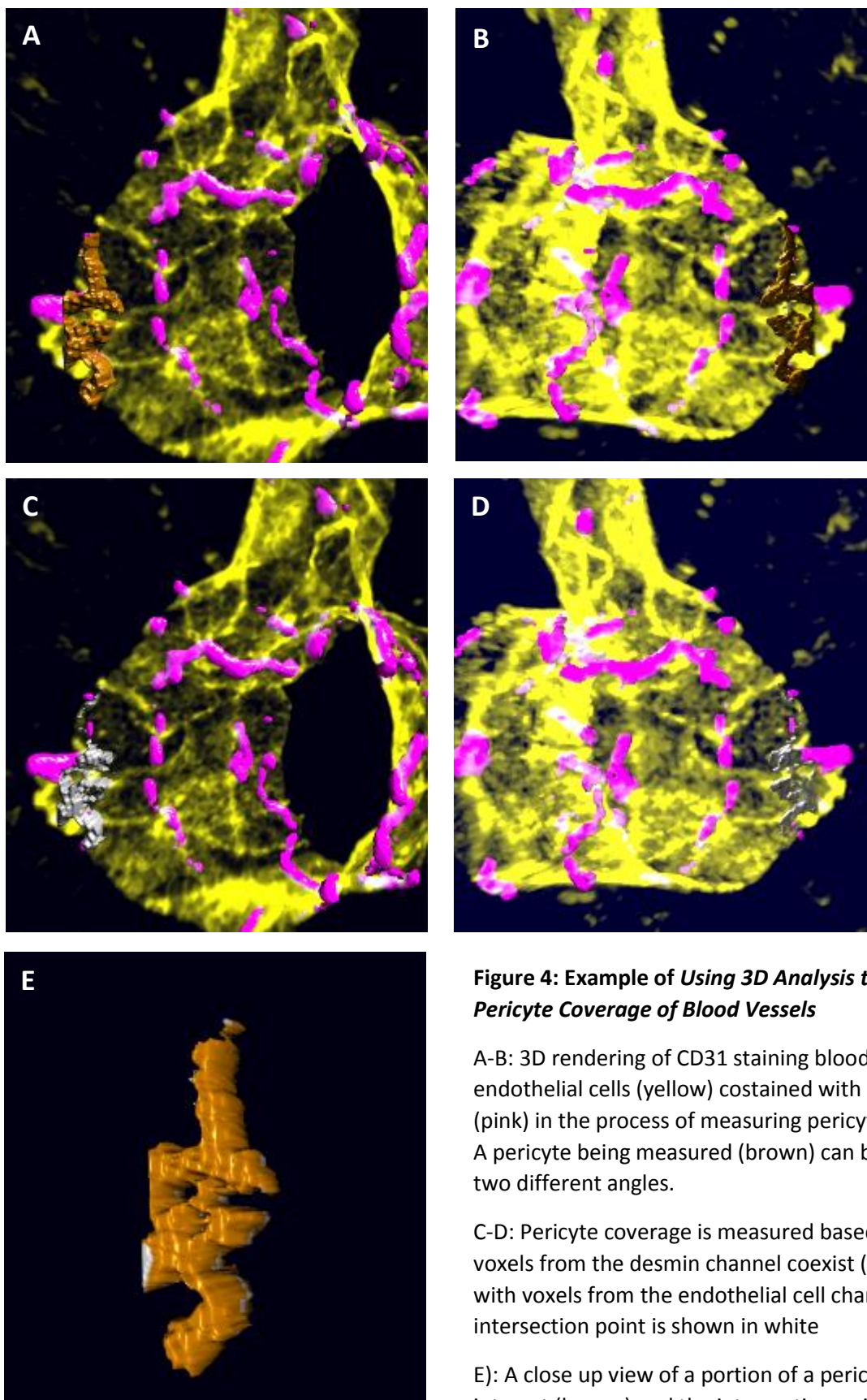


**Figure 4: Example of *Using 3D Analysis to Measure Pericyte Coverage of Blood Vessels***

A-B: 3D rendering of CD31 staining blood vessel endothelial cells (yellow) costained with Desmin (pink) in the process of measuring pericyte coverage. A pericyte being measured (brown) can be seen from two different angles.

C-D: Pericyte coverage is measured based on where voxels from the desmin channel coexist (intersect) with voxels from the endothelial cell channel. This intersection point is shown in white

E): A close up view of a portion of a pericyte of interest (brown) and the intersection point with the blood vessel to be measured (white) shows how a

***Astrocyte Points of Contact Measurement:***

In addition to measuring surface area of CD31 and GFAP intersection in Volocity, the amount of these contact points made was counted and totaled for each blood vessel simultaneously with the surface area measurements.

***Pericyte Volume Measurement:***

Total pericyte volume was measured in Volocity concurrently with the surface area analysis. The volume of the pericyte population detected from the desmin channel was measured to analyze the volume of the entire pericyte rather than just where the pericyte intersected with the blood vessel.

***Endothelial Cell Disruption Measurement:***

To measure the extent of any disruption of the endothelial cells and/or their tight junctions the ratio of the intact endothelial cells surface area to that of the whole blood vessels surface area was calculated. Surface area of the CD31 channel was measured from the entire blood vessel image. ROIs were drawn around areas where the distinct cobblestone pattern, marking the MVEC outlines were visible. The surface area of CD31 within these ROIs was measured. Ratios of the total intact endothelial cell surface area to that of the total blood vessel CD31 surface area were calculated from these measurements.

***Calculations and Statistical Analysis***

All additional data calculations and analysis were performed using Microsoft Excel and GraphPad Prism 6.

## Results:

### IHC Assay Development:

Approximately 30 different antibodies have been tested for both their sensitivity and specificity at detecting each component of interest in the BBB. Antibodies for the identification of astrocytes, pericytes, microglia and the basement membrane/extracellular matrix have been identified and fully optimized through a series IHC experiments to determine their ideal working concentration. All tested TJ protein specific antibodies however failed to produce positive results. Below is a detailed description of the IHC assay results and Table 4 presents a summary of all the antibodies that produced a positive signal and have been fully optimized for further experiments.

**Table 4: Working Antibodies**

| <b>Marker</b>            | <b>Antibody</b> | <b>Supplier/Catalog #</b> | <b>Host</b> | <b>Working</b> |
|--------------------------|-----------------|---------------------------|-------------|----------------|
| <b>Endothelial Cells</b> | CD31            | RD Systems/AF3628         | Goat        | 1:50           |
|                          | CD31            | Abcam/ab28364             | Rabbit      | 1:50           |
|                          | IB4             | Life Technologies/I21411  | N/A         | 1:100          |
| <b>Astrocytes</b>        | GFAP            | Sigma/SAB2500462          | Goat        | 1:1000         |
|                          | GFAP            | Sigma/ G3893              | Mouse       | 1:1000         |
|                          | GFAP            | Invitrogen/13-0300        | Rat         | 1:1000         |
| <b>Pericytes</b>         | Desmin          | Novus/NB120-1520          | Rabbit      | 1:100          |
|                          | αSMA            | Abcam/ab7817              | Mouse       | 1:100          |
|                          | αSMA            | Abcam/ab5694              | Rabbit      | 1:100          |
| <b>Microglia</b>         | IBA1            | Abcam/AB5076              | Goat        | 1:1000         |
| <b>Basement Membrane</b> | Collagen IV     | Millipore/AB769           | Goat        | 1:50           |
|                          | Collagen IV     | Abcam/ab19808             | Rabbit      | 1:500          |

### ***Endothelial Cell Markers:***

Antibodies were evaluated for both their sensitivity and their specificity to determine their overall effectiveness. Of the six reagents (5 antibodies and one probe) tested as markers for endothelial cells, three produced a positive signal. These three reagents include two antibodies, Goat anti-CD31 (RD Systems/AF3628) and Rabbit anti-CD31 (Abcam/ab28364), and the probe Isolectin B4- Alexa

488 (IB4). With all three reagents the staining pattern matching the branching of blood vessels of various sizes could be identified homogeneously across

the brain sections. Specificity refers to whether or not an antibody detects only its target antigen. Optimization experiments, using the antibodies at various concentration levels were performed to test each antibodies specificity and to find their ideal signal to noise ratio. In these experiments, both CD31 antibodies despite producing the proper staining patterns at concentration ratios

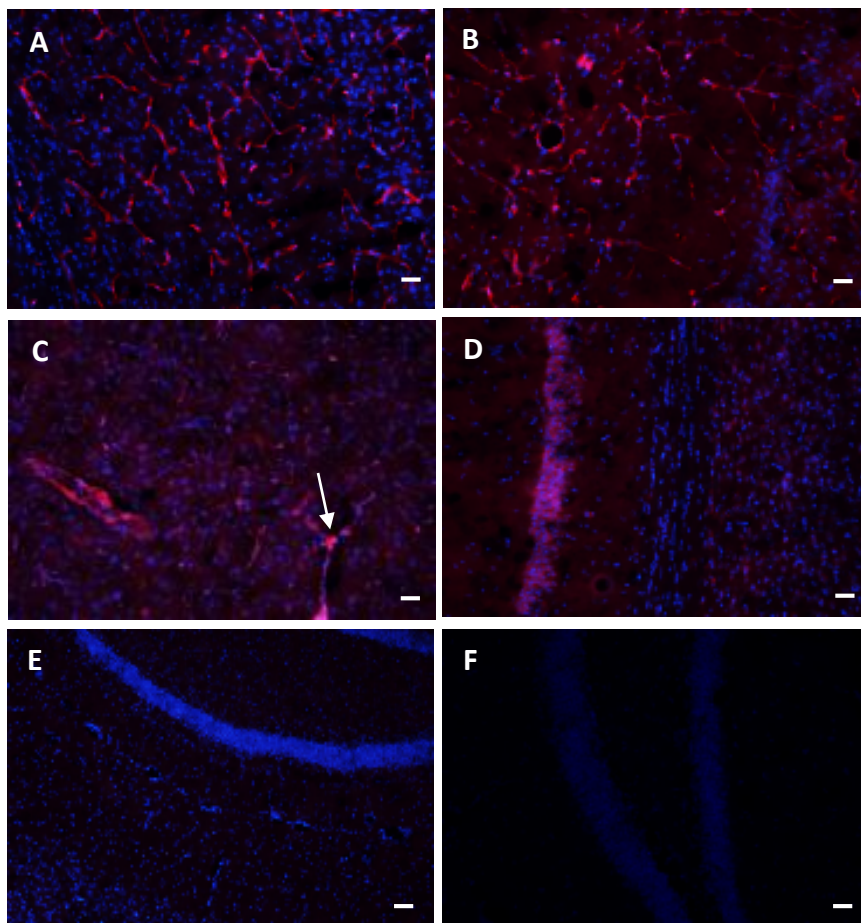


**Figure 5: Immunohistochemical Assay Development of Endothelial Cell Markers** A) Goat anti CD31 (RD Systems/AF3628) optimized at a concentration of 1:100 produces a strong signal to noise ratio with the correct blood vessel staining pattern. An example of ideal antibody sensitivity and specificity. B) Rabbit anti CD31 optimized at 1:50 also produces a good signal to noise ratio and correct staining pattern. C) Isolectin B4-AlexaFluor 555 optimized at 1:100 stains blood vessels and microglia (arrow) thus demonstrating a lack of specificity required for image analysis. D-E: In order Rabbit anti CD31 (Sigma/SAB4502167), Rat anti CD31 (Millipore/CBL1337), and Rat anti CD31 (Abcam/ab56299). All three images have no positive signal and demonstrate the results of antibodies with poor sensitivity. All images are taken at a 10x objective, scale bars 20  $\mu$ m.

ranging from 1:10 to 1:1000 also produced a high background signal that could not be avoided without increased wash times. As a result the general IHC protocol described above was adapted to increase wash number and duration after antibody incubations from 1 hour to 4 hours with multiple changes of buffer. These optimization experiments found that the working concentration ratio for the Goat anti-CD31 antibody was 1:500 and the Rabbit anti-CD31 was 1:50 (Fig. 5). Isolectin B4 (IB4), a lectin that has been used to label endothelial cells in tissue was found to indeed stain blood vessels but also produced a strong signal in microglia, as has been previously described, thus lacked the specificity needed for adequate image analysis and was eliminated as a blood vessel marker. All other blood vessel markers tested did not produce a positive signal at the sensitivity testing stage (Fig. 5).

### *Astrocyte Markers*

Three antibodies were tested and successfully optimized as astrocyte markers. These antibodies were Goat anti-GFAP (Sigma/SAB2500462), Mouse anti-GFAP (Sigma/ G3893) and Rat anti-GFAP (Invitrogen/13-0300). All three antibodies were tested for sensitivity and specificity similar to the endothelial cell markers and all three produced a satisfactory signal to noise ratio at concentration ratios of 1:1000. During image analysis, positive staining of astrocytes was confirmed by visualization

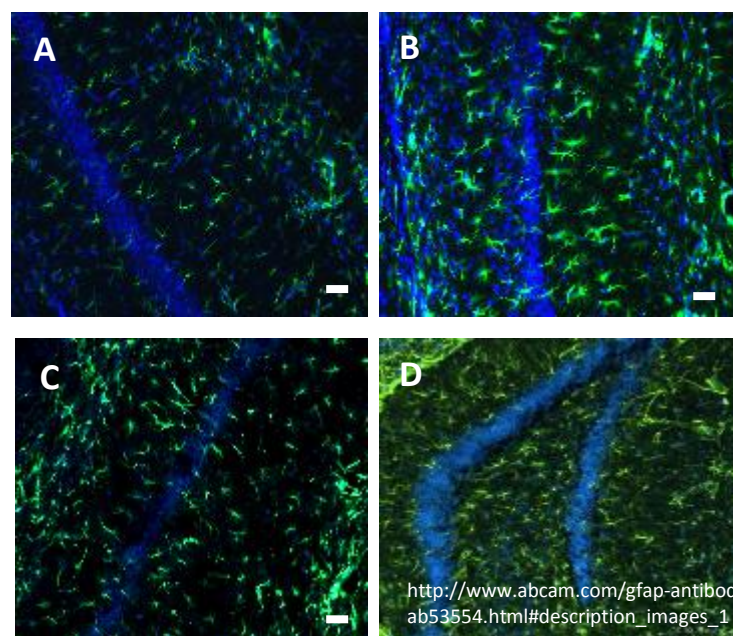


**Figure 6: Immunohistochemical Assay Development of Astrocyte Markers.** A) Goat anti GFAP (Sigma/SAB2500462). B) Rat anti GFAP (Invitrogen/13-0300). C) Mouse anti GFAP (Sigma/ G3893). D) Image provided by Abcam as an example of a positive GFAP signal. All three antibodies (A-C) produce a staining pattern consistent with that in D and can therefore be confirmed to produce a positive signal. The antibodies in A-C have all been optimized to work at 1:1000 with minimal background staining. Scale bar = 20  $\mu$ m.

of the star shaped morphology of the astrocyte body with its many foot process as well as the organized non-overlapping orientation of the astrocytes (Fig. 6). Additionally, when all GFAP antibodies were costained with an endothelial cell marker, the end feet of the astrocytes were clearly observed to be adjacent to against the blood vessel wall as has been previously described (Fig.7).

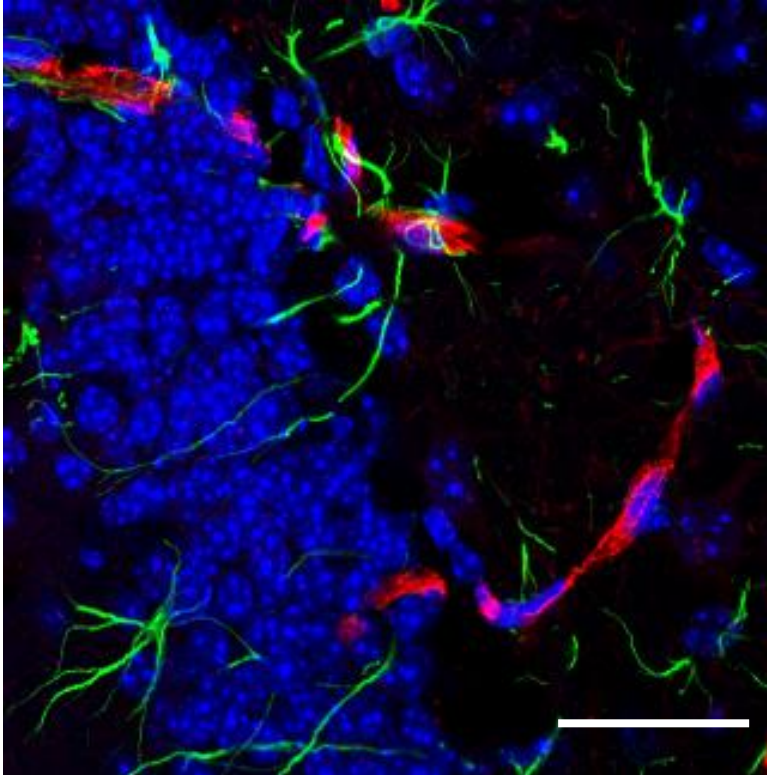


**Figure 7: GFAP Costained with CD31 Illustrates Astrocyte Interactions with Blood Vessels**

When costained with CD31 (red), GFAP (green) can be seen to positively stain astrocytes as they interact with blood vessels. Image was acquired using a confocal microscope in order to capture the detail of the astrocyte foot processes in contact with the blood vessel. Scale bar = 20  $\mu\text{m}$ .

### *Pericyte Markers*

Out of the eight different pericyte markers that were tested and only three were determined to provide appropriate staining

patterns: rabbit anti-desmin (Novus/NB120-15200), mouse anti-alpha smooth muscle actin (ASMA) (Abcam/ab7817), and rabbit anti-ASMA

(Abcam/ab5694). All other antibodies listed in Table 1 did not produce the appropriate staining pattern and were not pursued further. When tested for specificity all three antibodies produced a high signal to noise ratio and the working concentrations were determined to be 1:100 for all three (Fig. 8). A positive pericyte signal was further confirmed for each of the working

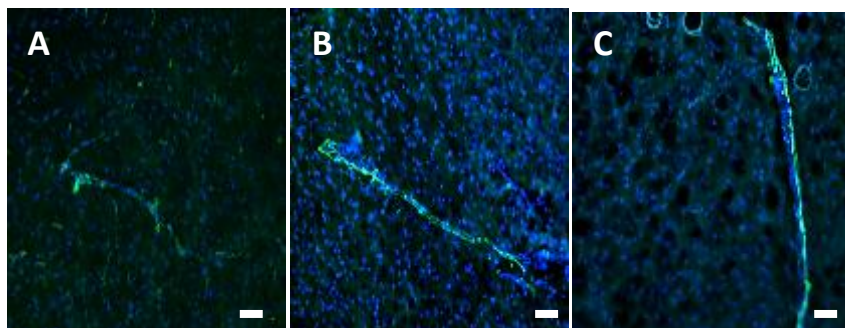
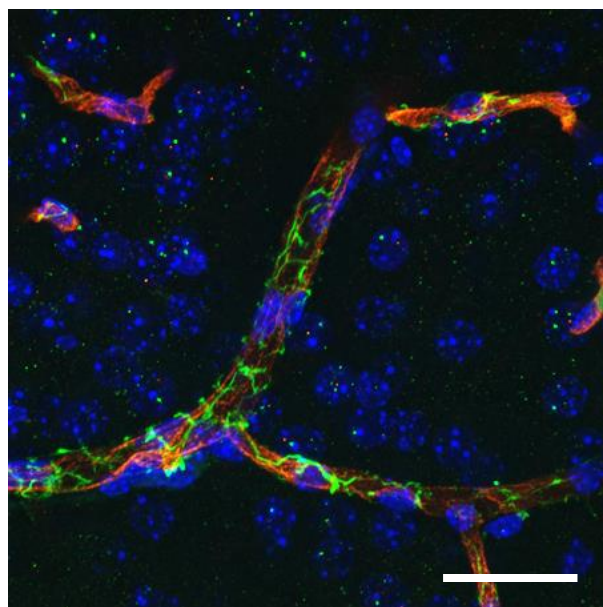


**Figure 8: IHC Assay Development of Working Pericyte Markers**

A) Rabbit anti Desmin (Novus/NB120-1520), B) Rabbit anti Alpha Smooth Muscle Actin (Abcam/ab5694), and C) Rabbit anti Alpha Smooth Muscle Actin represent the three potential pericyte markers that produced a positive signal. The other five antibodies (not pictured) failed to produce a signal. Even without a blood vessel the staining pattern can be seen to correspond with the location of blood vessels giving support that these antibodies are detecting pericytes. Desmin (A) appears to produce signal in smaller vessels as well as larger where as smooth muscle actin (B-C) appears limited to larger vessels. Scale Bar = 20  $\mu$ m.



antibodies by a costain with a CD31 antibody. The pericyte staining was morphologically confirmed with confocal microscopy (Fig. 9).

**Figure 9: Confocal Image of a Desmin and CD31 Antibody Costain Confirms Pericyte Marker**

Desmin (green) is confirmed in this costain with CD31 (red) to be functioning as a pericyte marker based off both its association with endothelial cells and the morphology of the processes wrapping around the vessel. Scale bar = 20  $\mu$ m.

### ***Microglia Marker***

One antibody was tested as a microglia marker, Goat anti Iba1 (Abcam/AB5076). This antibody proved to be sensitive and specific at detecting microglia at a working concentration ratio of 1:1000. The microglia were detected by their unique ramified shape, most common throughout the brain, consisting of a small cell body and long branching processes (Fig. 10).

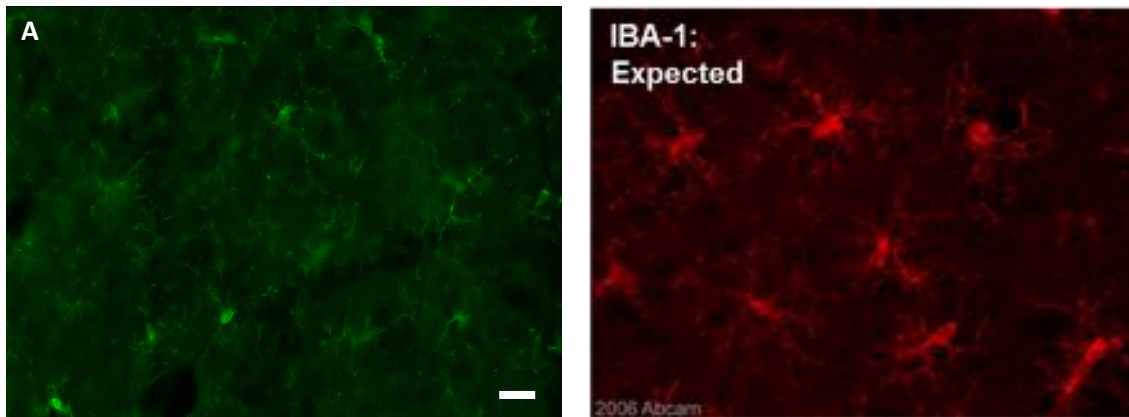


**Figure 10: IHC Assay Development of IBA1 as a Microglia Marker**

A) Goat anti IBA1 (Abcam/AB5076) optimized at 1:1000 compared to the image provided by the supplier Abcam of the expected staining results of this antibody. This antibody matches the staining pattern of the expected results as well as the known staining pattern of microglia in the CNS including the small cell body and long branching arms. Scale bar = 20  $\mu$ m.

### ***Tight Junction Markers***

Several tight junction markers were tested and retested however none have been determined to detect tight junction proteins at this point. However, CD31 also known as platelet endothelial cell adhesion molecule (PECAM) has been reported to be expressed in the TJs of endothelial cells<sup>10,51</sup>. This cobblestone TJ staining pattern was observed with both CD31 (PECAM) antibodies when used at their optimal concentrations (Fig. 11).

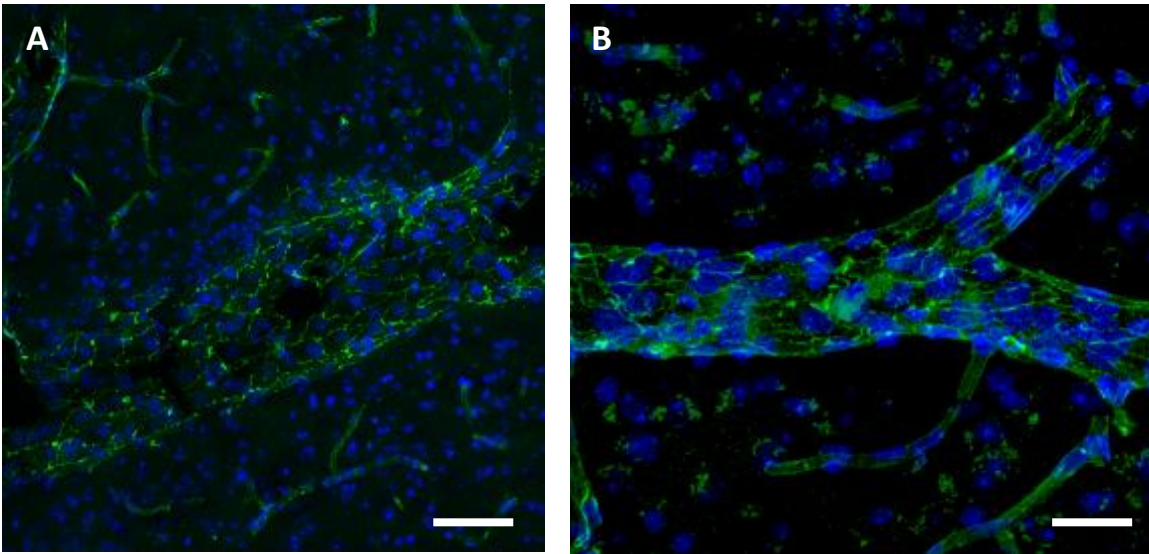


**Figure 11: Anti CD31 Antibodies Functions as a Tight Junction Marker** A-B represent confocal images of two different blood vessels stained with CD31 (green). Positive CD31 signal can be seen brightest as outlines (junctions) of endothelial cells that line blood vessels. CD31 has been reported to be localized in the tight junctions of the endothelial cells these images give evidence to support these reports and suggest that CD31 will work as a marker for tight junction integrity in future experiments. Scale bar = 20  $\mu$ m.

### ***Basement Membrane Markers***

Two antibodies have been tested as a basement membrane marker: Goat anti-Collagen IV (Millipore/AB769) and Rabbit anti-Collagen IV (Abcam/ab19808). Visually at first, the basement membrane staining pattern looks similar to that of the blood vessel markers, however, the basement membrane ensheathes the endothelial cells and therefore can be seen as the outer layer when costained with an endothelial cell marker. Of the two antibodies tested, the Goat anti-Collagen IV produced the most sensitive and specific staining pattern of the two with a working concentration ratio for 1:50. The rabbit anti-collagen IV antibody still produced good sensitivity and specificity at 1:500.

### ***Blood Vessel Classification by Average Diameter Calculation:***

Blood vessels were grouped into categories based on their calculated average diameter from the measured cross section area of each slice in the blood vessel image z-stack. Before the

blood vessels could be categorized however, the measurement results were quality checked to confirm that the areas measured matched the imaged blood vessel cross section and that a minimum of 10 slices in each z-stack were measured. If a blood vessel image did not meet both minimum requirements the image was classified as failing the QC process and not included in further analysis.

Blood vessels that passed the QC process were categorized based on their average calculated diameter per region and per animal using size guidelines taken from literature<sup>46</sup> (Table 5).

**TABLE 5: MICROVESSEL CLASSIFICATION BY DIAMETER SIZE**

|   |  |
|---|--|
| <b>&lt; 10 <math>\mu\text{m}</math></b> | <b>Capillary</b>   |
| <b>11-20 <math>\mu\text{m}</math></b>   | <b>Pre-Capillary Arterioles</b><br><b>Post-Capillary Venules</b> |
| <b>&gt; 20 <math>\mu\text{m}</math></b> | <b>Arterioles/Venules</b>  |

Tables 6 and 7 provide the numerical classification of blood vessels in each size group for the cortex and thalamus of the WT and MPS IIIB mice respectively. While vessels were categorized into four different groups only vessels that fell into groups one and two were used in further analysis.

**Table 6: Cortex Blood Vessel Categorization**

| <i>Genotype</i>    | <i>Animal Name</i> | <i>Capillaries<br/>&lt; 10 <math>\mu\text{m}</math></i> | <i>Pre and Post<br/>Capillary<br/>Arterioles and<br/>Venules<br/>11-20<math>\mu\text{m}</math></i> | <i>Arterioles and<br/>Venules<br/>&gt; 20 <math>\mu\text{m}</math></i> |
|--------------------|--------------------|---|--|--|
| <b>WT</b>          | WT-1 Cortex        | 20  | 14   | 1  |
|                    | WT-2 Cortex        | 21  | 9  | 2  |
|                    | WT-3 Cortex        | 30  | 5  | 0  |
|                    | WT-4 Cortex        | 17  | 7  | 1  |
|                    | WT-5 Cortex        | 8   | 4  | 0  |
| <b>MPS<br/>IIB</b> | MPS IIB-1 Cortex   | 17  | 8  | 0  |
|                    | MPS IIB-2 Cortex   | 18  | 5  | 0  |
|                    | MPS IIB-3 Cortex   | 11  | 10   | 0  |
|                    | MPS IIB-4 Cortex   | 21  | 6  | 0  |
|                    | MPS IIB-5 Cortex   | 23  | 6  | 0  |

**Table 7: Thalamus Blood Vessel Categorization**

| <i>Genotype</i>    | <i>Animal Name</i>    | <i>Group 1:<br/>Diameter<br/>&lt; 9 <math>\mu\text{m}</math></i> | <i>Group 2:<br/>Diameter 9-13.5<br/><math>\mu\text{m}</math></i> | <i>Group 4: Diameter &gt;<br/>20 <math>\mu\text{m}</math></i> |
|--------------------|-----------------------|--|--|---|
| <b>WT</b>          | WT-1 Thalamus         | 15   | 17   | 4   |
|                    | WT-2 Thalamus         | 24   | 7  | 2   |
|                    | WT-3 Thalamus         | 21   | 13   | 0   |
|                    | WT-4 Thalamus         | 12   | 13   | 4   |
|                    | WT-5 Thalamus         | 13   | 7  | 0   |
| <b>MPS<br/>IIB</b> | MPS IIB-1<br>Thalamus | 15   | 19   | 5   |
|                    | MPS IIB-2<br>Thalamus | 19   | 13   | 3   |
|                    | MPS IIB-3<br>Thalamus | 16   | 12   | 2   |
|                    | MPS IIB-4<br>Thalamus | 21   | 15   | 0   |
|                    | MPS IIB-5<br>Thalamus | 20   | 16   | 2   |

***Correlation of 2D Vessel Area Measurement Vs 3D Vessel Area Measurement Confirms Improved Accuracy of 3D Analysis***

Initial image analysis provided first hand evidence to support literature claims that 2D blood vessel diameter measurements results in inaccurate data (Fig. 1). As a result of these early findings and literature reports, extensive work was done to develop the protocol used in this project with the goal accurately measure blood vessel cross sectional areas in 3D. In addition to the control stacks measured, confirmation that 3D analysis of blood vessel cross sectional areas is advantageous over 2D analysis was assessed by taking a single slice representing the apparent cross sections from 32 blood vessel image stacks at random to undergo analysis using traditional 2D methods. Each chosen image slice was analyzed by manually making a line measurement across each vessel's apparent diameter and calculating the area from it. The results of this measurement were then graphed versus the 3D measured areas of the same vessels. The results of this comparison gave an  $r^2$  value of 0.008616 showing very little correlation between the two measurement methods (Fig. 12). Additionally when maximum projections\* of the blood vessel image stacks were composed they showed the apparent vessel diameters measured were not accurate representations of the blood vessel diameters as predicted (Fig. 13).

## 2D Vs. 3D Vessel Area Measurement

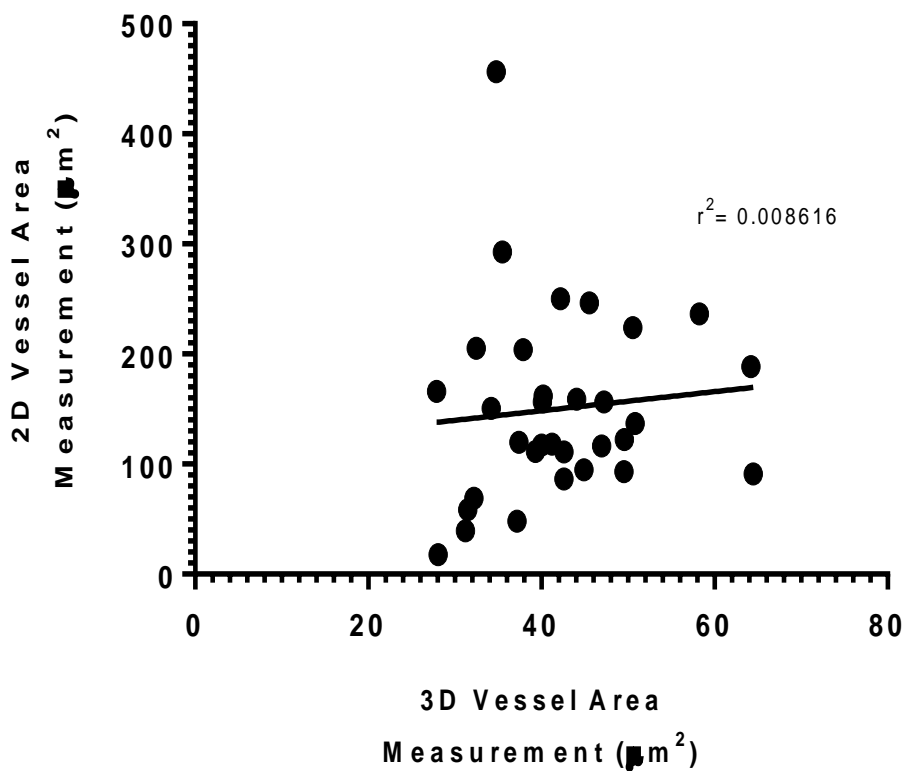


**Figure 12: No Correlation Between 2D and 3D Blood Vessel Area Measurement Protocols:**

Results of blood vessel cross sectional area were measured using both traditional 2D line measurements and 3D analysis to help confirm the inaccuracies of 2D analysis. When the results of the two analysis methods were plotted against each other no correlation was observed to help confirm the necessity of 3D analysis

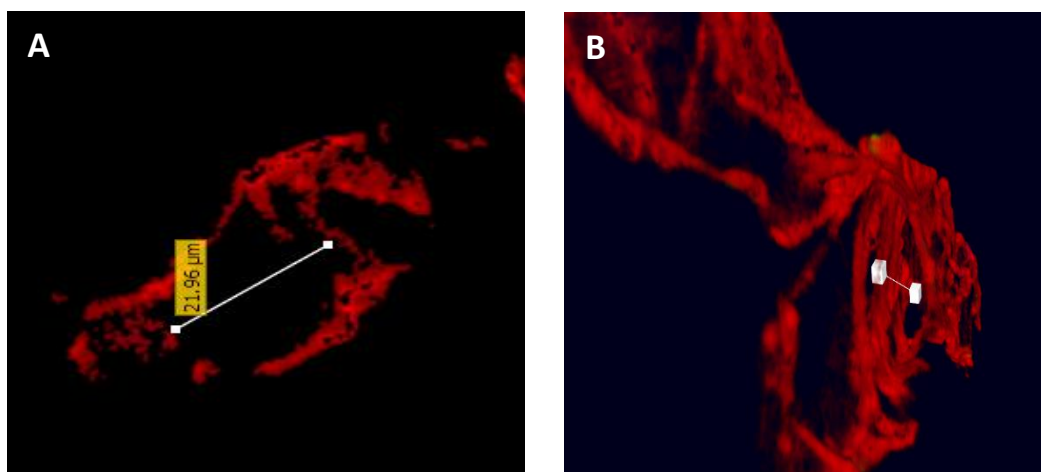


**Figure 13: Traditional 2D Blood Vessel Measurement Results in Inaccurate Characterizations** Apparent cross section line measurement in a 2D image slice (A) compared to the maximum projection of the entire blood vessel image stacks(B) highlights the inaccuracies of 2D vessel characterization and provides support for the need for 3D analysis.

### ***Changes in Astrocyte Foot Process Coverage of MVECs:***

The changes in astrocyte foot process contact with MVECs was analyzed by measuring the surface area ( $\mu\text{m}^2$ ) of the coincidence of the GFAP and CD31 signals in Velocity. The total sum surface area ( $\mu\text{m}^2$ ) of this astrocyte-blood vessel interaction was calculated per blood vessel and then averaged per animal. In the capillaries there was a significant increase in astrocyte-blood vessel contact area interactions and a trending increase in the thalamus. In the larger pre and post capillary vessels we also saw this trending increase (Fig. 14).

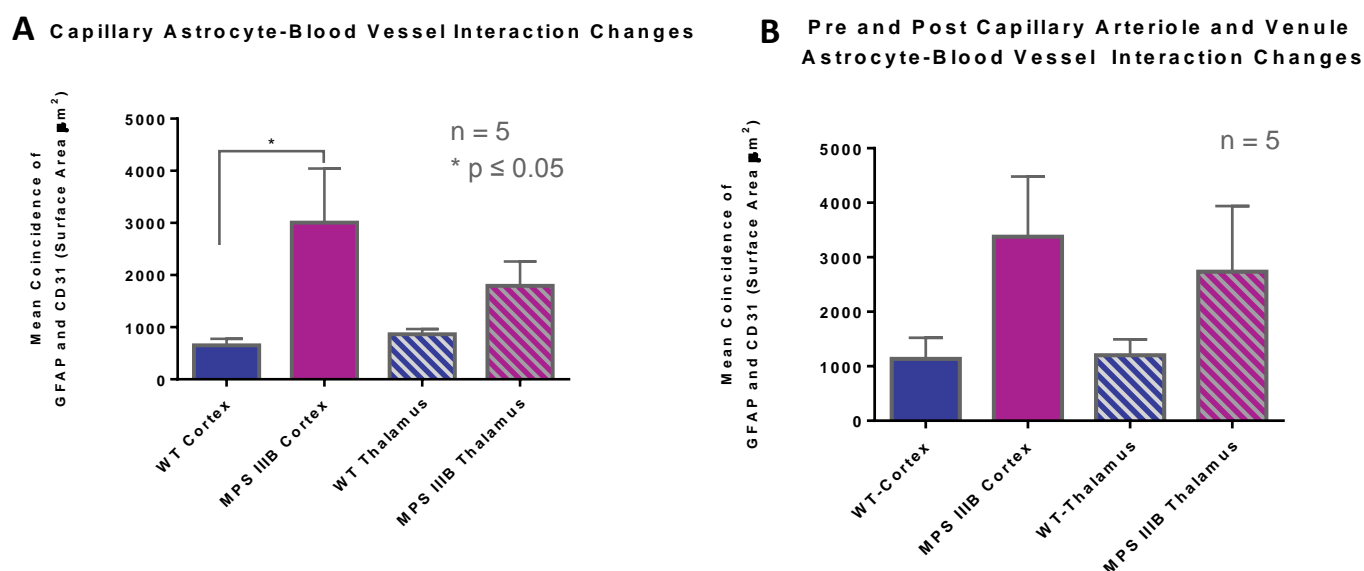


**Figure 14 Analysis of Astrocyte and Blood Vessel Interaction Changes in WT and MPS IIIB Mice.**

A) Capillary results of measuring the point of intersection of the CD31 and GFAP signals ( $\mu\text{m}^2$ ) show significant increase in astrocyte foot process contact with MVECs and a trending increase in the thalamus. B) Pre and post capillary also show a trending increase astrocyte-blood vessel contact area.

### ***Changes in Astrocyte Foot Process Contact Points with MVECs:***

Astrocytes are thought to give instructions to endothelial cells through their end feet contact points. Therefore we additionally, measured how many points of contact the astrocytes made with the endothelial cells. We observed a significant increase in contact points in capillaries from both the cortex and the thalamus in MPS IIIB compared to WT mice. While the

increase for the larger vessels remained statistically not significant it did continue to show the upward trend in contact (Fig. 15).

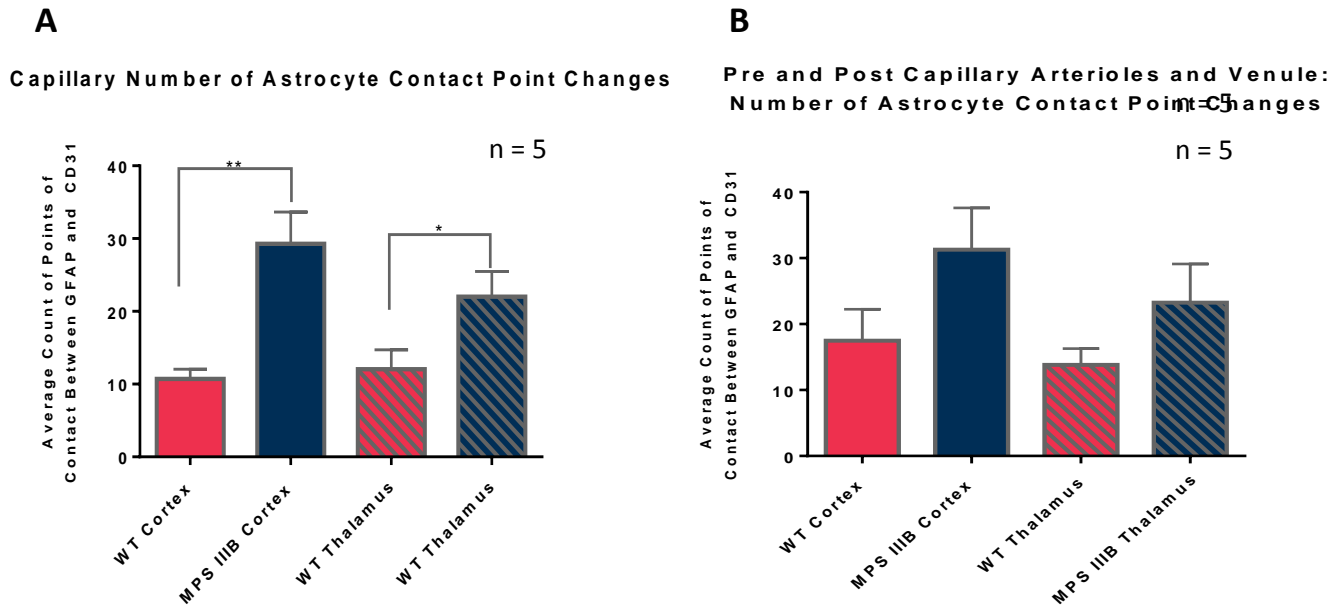


**Figure 15 Analysis of Astrocyte and Blood Vessel Interaction Changes in WT and MPS IIIB Mice.**

A) Measurements of the total points of contact where CD31 and GFAP signals intersect in the capillaries show significant increase in astrocyte foot process contact with MVECs in both the cortex and the thalamus. B) Pre and post capillary also show a trending increase in astrocyte foot process contact with the blood vessels

#### **Comparison of Pericyte Coverage of MVECs:**

Pericyte coverage of MVECs were measured using the same method described for analyzing astrocyte foot process contact. The pericyte-blood vessel interactions were measured from the coincidence of desmin and CD31 signals and the surface area was measured and analyzed in the same way described for the astrocyte-blood vessel interactions. No significant change was observed in the surface area in these desmin positive pericytes in any region or blood vessel grouping between WT and MPS IIIB animals (Fig. 16).

### *Analysis of Pericyte Volume Between WT and MPS IIIB*

In addition to measuring the surface area of where desmin and CD31 intersected the volume of the total desmin signal was measured as well in order to determine if pericytes were swollen as suggested in literature<sup>31</sup>. No difference between WT and MPS IIIB pericyte volume was observed for either blood vessel group in both the cortex and the thalamus contrary to what was previously reported<sup>31</sup> (Fig. 17).

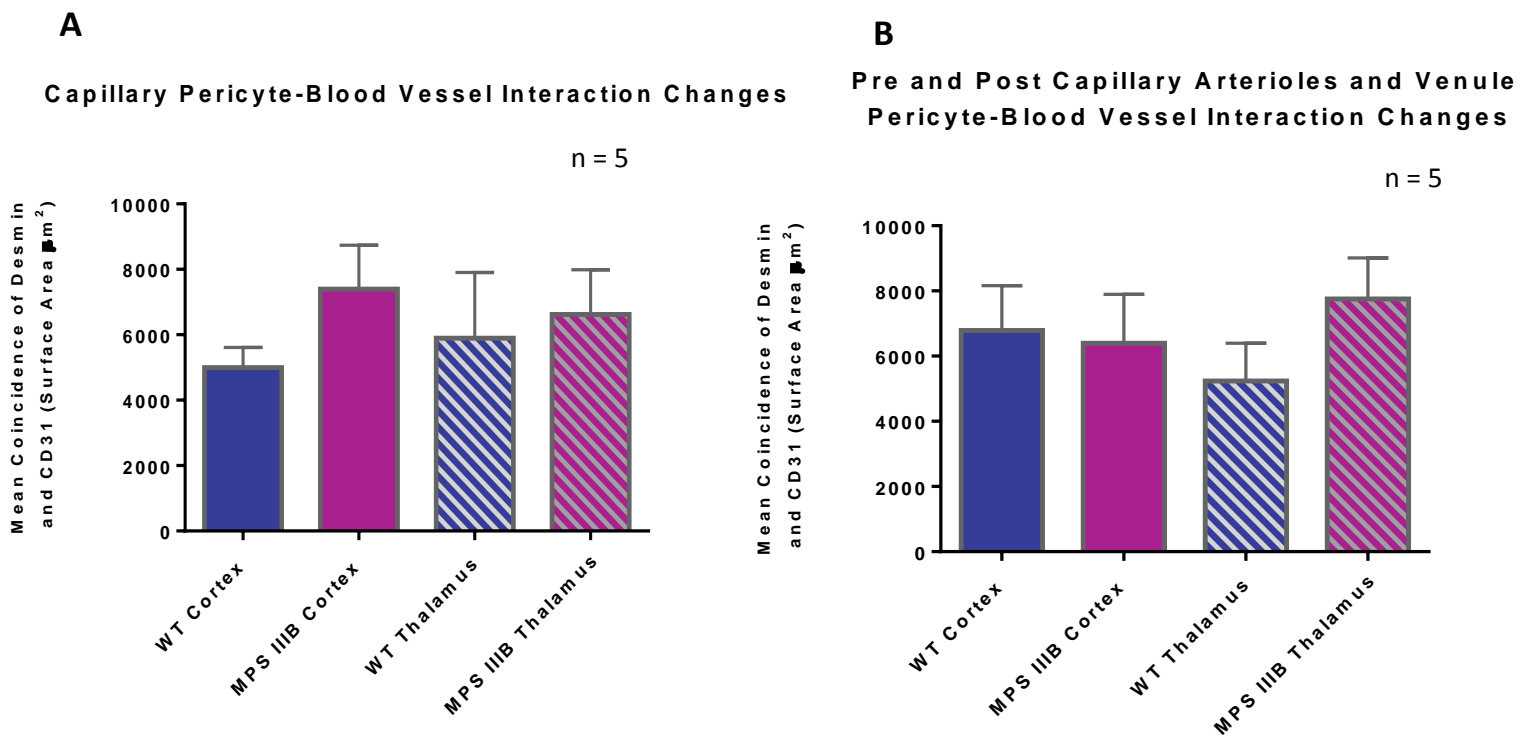


**Figure 16 No Significant Changes in Surface Area Measurement of Pericyte Intersect Population** No change in pericyte contact area between MPS IIIB and WT mice in the capillaries (A) or for the pre and post capillary vessels (B) of either the cortex or the thalamus.

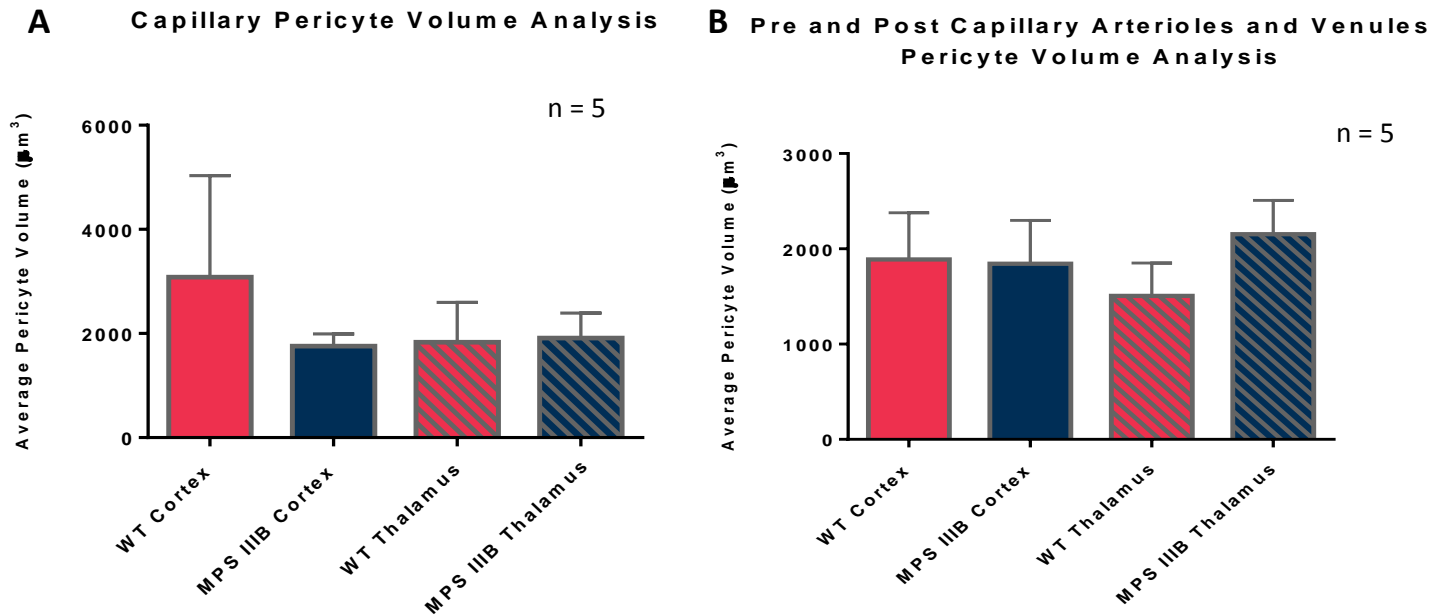


**Figure 17 Analysis of Desmin Positive Pericyte Volume in WT and MPS III B Microvasculature** No change in pericyte volume between MPS III B and WT mice in the capillaries (A) or the pre and post capillary vessels (B) of either the cortex or the thalamus. Suggests no increase in swelling of the pericytes in MPS III B mice as reported in literature.

### *Assessing Endothelial Cell Damage In MPS III B*

Literature reports suggested endothelial cell damage in MPS III B<sup>31</sup>. Utilizing CD31 to visualize endothelial cells and their tight junctions we were able to visually confirm disruption to the endothelial cells suggesting tight junction damage.(Fig. 18). When quantified we observed a significant decrease in the percent of intact endothelial cells in capillaries from MPS III B mice compared to those in WT mice (Fig. 19)

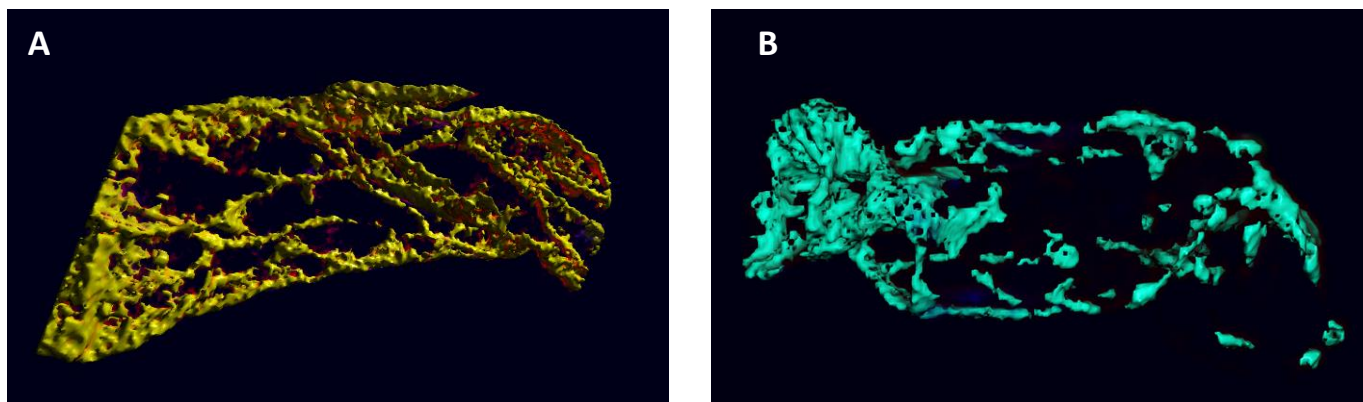


**Figure 18 Comparison of Endothelial Cells in WT and MPS III B Mice Show Endothelial Cell Disruption** A) A WT capillary with intact endothelial cells and undamaged tight junctions. B) An MPS III B capillary with disrupted endothelial cell damage equated to tight junction damage.

#### Average Intact Endothelial Cells/Tight Junctions Analysis

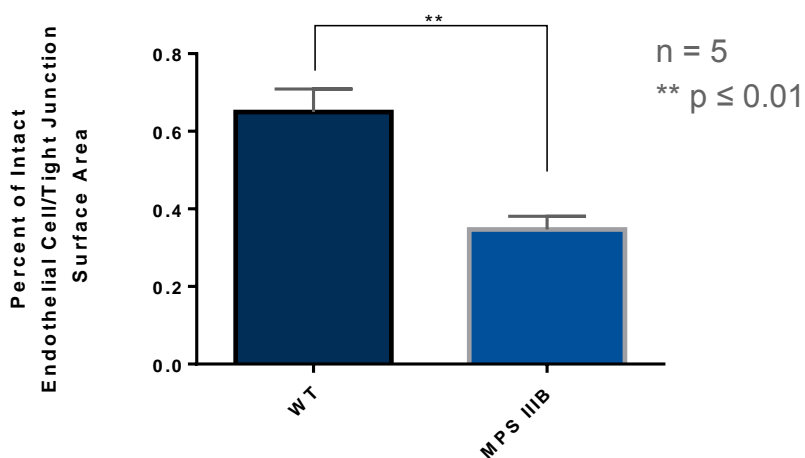


**Figure 19 Quantification of Endothelial Cell Disruption** The percent of intact endothelial cells in MPS III B mice was measured in 10 randomly selected capillaries from the cortex of each animal in WT and MPS III B. A significant decrease in the amount of undamaged endothelial cells in MPS III B capillaries of the cortex was observed compared to WT

## **Discussion:**

The overall purpose of this project was to develop the tools and techniques needed to create a quantitative model of the BBB in normal adult mice that would then allow for the evaluation of the effects of development and disease on the BBB. To accomplish this goal, each component of the BBB was examined through immunohistochemistry, confocal microscopy, and 3D image analysis in order to quantify their relationship with the MVECs. The initial stages were focused on optimizing an IHC protocol that would produce high quality staining of blood vessel endothelial cells in thick tissue sections costained with various other antibodies to identify the components of the BBB. A standard IHC experiment typically uses tissue sections 5-10  $\mu\text{m}$  in thickness, however, in order to capture full cross section diameters of blood vessels, thicker tissues of 50  $\mu\text{m}$  were utilized. To maximize penetration of antibodies into these thicker tissue samples a staining protocol was developed using a floating tissue technique, rather than the more common method of staining tissues while mounted on a slide. This allowed the antibodies to have access to both sides of the tissue, increasing the depth of antibody penetration. Furthermore washing in this manner also was more effective in removing unbound antibody which can cause unwanted background signal.

The significant finding of this project was support for the hypothesis that traditional 2D blood vessel analysis is indeed an inaccurate and invalid approach. The development of a 3D protocol was a monumental task that took several different approaches before settling on the one used. The requirements set in place this measurement protocol included that it must be efficient, accurate, reproducible, and would work with various blood vessel sizes and shapes. Additional considerations included that the protocol require minimal computing power and also be automated but these were not considered requirements. Early measurement protocol ideas

included the traditional 2D blood vessel diameter line measurement, which was quickly demonstrated to be inaccurate (Fig. 1 and Fig. 13). A second approach attempted was to measure the skeletal diameter of the blood vessels in Volocity which calculates the diameter based off the volume of a cylinder with the same volume and maximum length as the measured blood vessel. This method was determined to be inadequate as it relied too much on the maximum length of the blood vessel. The maximum length was calculated automatically by Volocity and was not always a straight line from one end of the vessel to the other, but rather would twist and turn throughout the volume depending on where the highest voxel intensity was localized. The skeletal diameter approach led to the idea that an accurate diameter could be calculated from the volume of the blood vessel, using the formula for the volume of a cylinder, if the proper length of the blood vessel was measured. However, again this method was discarded due to the inability to reproduce accurate results which varied too much depending on the length, shape and volume of the blood vessels. The final attempted measurement protocol went back to the basic concepts of the 2D measurement approach, but rather than making a line measurement at one focal plane, line measurements across the apparent diameters were made in every slice of the image stacks and then averaged. The advantage idea behind this approach was the idea that measuring through the entire image stack would account for all the changes that occur to the diameter size throughout the length of the blood vessel. However, the limitations to this approach included the length of it took to manually draw an accurate line in every image slice in stacks that averaged 150 slices. Secondly, the results from this approach were sensitive to the subjective decision of where and how the line measurement was drawn. For example, rarely do blood vessel cross sections appear as a perfect circle, more often they behave more as an ellipse with major and minor diameter axis, measuring the diameter along only one axis could potentially skew data

results inaccurately. Based on these results it was then hypothesized that a simple line measurement whether it be in a single focal plane or averaged through an entire z-stack still would not provide the accuracy desired. To solve these issues we instead measured the average cross-sectional area of blood vessel image stacks as a way to determine the average diameter.

The protocols and assays developed in this project, particularly for the blood vessel characterization, were not possible until the last few years. Advances in both microscope and image analysis technologies have allowed for the hundreds of images and blood vessels required for this projects analysis to be analyzed in weeks rather than months or years, but room for advancement still exists.

Commercial 3D software programs such as, Volocity, offer a user-friendly interface to produce high quality 3D image visualization, as well as analysis tools. Unfortunately, the quantification power of these software can be limited by the scope of the software programming they are installed with. What Volocity and other recently developed 3D software systems lack is the customizability of the commonly used, open source, java language based ImageJ. The ability to adapt ImageJ processing functions to specific processing needs through custom built macros and plugins creates a much more powerful image processing platform. In order to make full use of the advantages of ImageJ however, a basic understanding of its programming language, Java, is necessary. Additionally, ImageJ was developed for 2D image processing and while 3D plugins exist and are beginning to advance, they lack the straightforward ease of use of the commercial products.

As a result of the various benefits and shortcomings of the available image processing software available a combination of the both Volocity and ImageJ were required in order to measure and classify the imaged blood vessels by their cross sectional area. By combining these

two image processing programs, a unique methodology for blood vessel classification was developed. The major advantage of utilizing Volocity for the initial image processing is the ability to visually rotate the 3D structure around its axis until the vessel's cross section is aligned with the xy plane of the image. The reslice function in Volocity allows a new 3D blood vessel image in the desired orientation to be reconstructed in the orientation set by physically moving the original 3D blood vessel representation. The advantage of this method over the method offered in ImageJ is the ability to visualize in 3D how the vessel's cross section is aligned with the xy image plane. In ImageJ users must know and input the x, y, and z angles that they wish the image to be aligned at without visual aid making this analysis more laborious.

As beneficial as Volocity is for 3D visualization and reorienting blood vessels there are limitations in evaluating the cross sectional area or diameters of resultant blood vessels in 3D. Therefore, images were exported into ImageJ so they could be analyzed using the custom written area measurement macro created for these image stacks. The macro allowed the area within the vessel walls to be measured in every slice of an image stack and furthermore could be batch processed to automatically measure every blood vessel image stack in a designated folder. Requirements set to avoid incorrect object detection and thus false measurements included setting a minimum area requirement of  $25 \mu\text{m}^2$ . Additionally, in order to be detected as an object, not background, the blood vessel wall had to be completely enclosed, otherwise no measurement would occur. Therefore, to improve the chances of a measurement occurring the open command was added to the measurement macro to close any small gaps in the vessel wall without altering the shape of the vessel cross section.

As a result of these measurement requirements approximately 60-70% of blood vessel images end up being eliminated from further analysis before they were categorized into their

different size classifications. To overcome this severe drop off in eligible blood vessels approximately 150-200 images were acquired per animal in order to reach a minimum of 10 eligible blood vessels per category. Traditionally, the requirement of hundreds of large z-stack images would take weeks of around the clock imaging. However, advances in microscope technology, specifically with the Leica SP8 LSM, made it possible to image approximately 100 z-stacks in 1-4 hours depending on acquisition settings. Therefore, by taking advantage of advancing image acquisition and processing technologies an accurate method of characterizing blood vessels by cross section area was created which overcomes the shortcomings of traditional 2D measurements (Fig. 20).

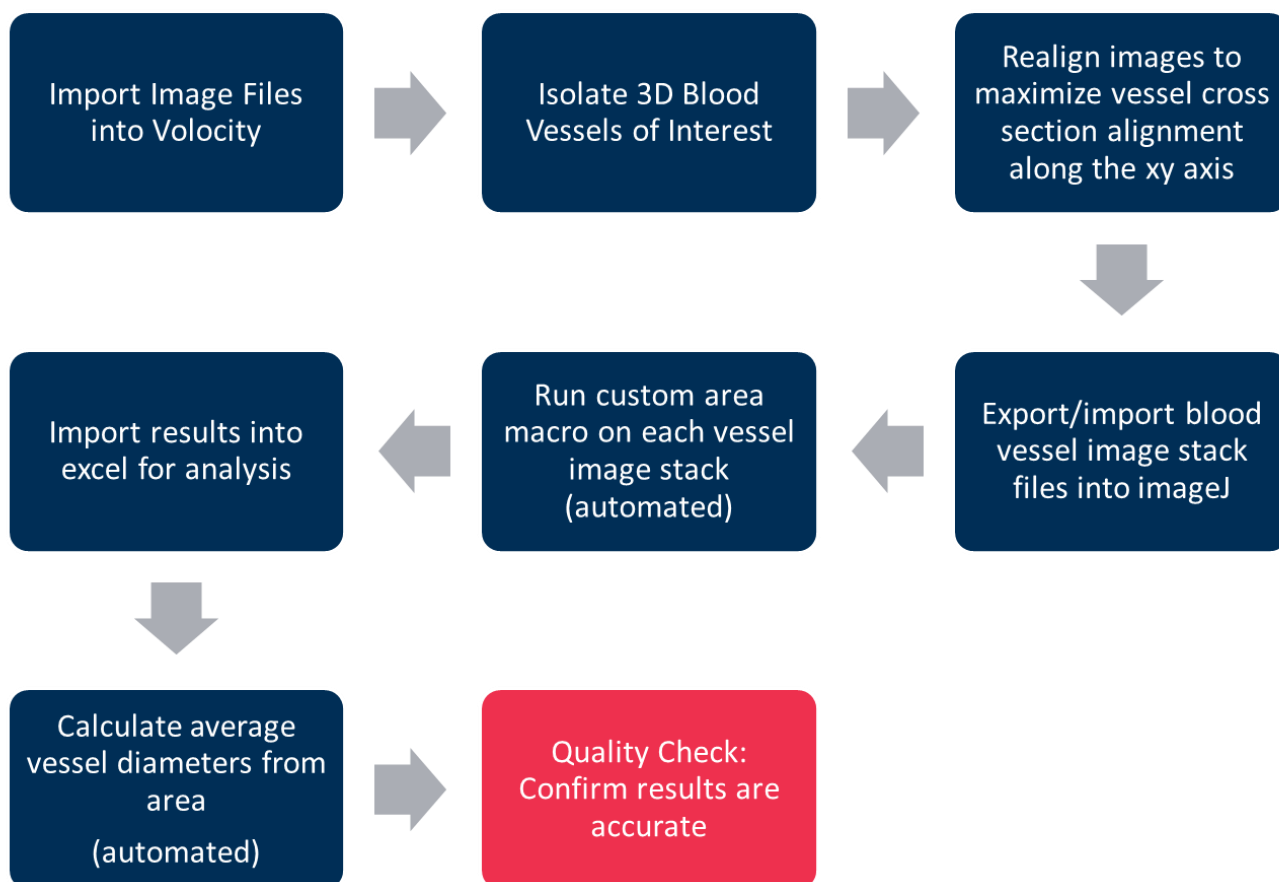


**Figure 20 Summary of Blood Vessel Classification Process**

Once blood vessels were measured and categorized with their size classifications blood vessels capillaries ( $< 10 \mu\text{m}$ ) and pre and post capillary arterioles and venules ( $11\text{-}20 \mu\text{m}$ ) were used in analysis to study changes in both astrocyte foot process and pericyte coverage of the MVECs. These two vessel groups have the most significant BBB function as well as make up the majority of vascular surface area within the brain. In Volocity, the resliced blood vessel images underwent a measurement protocol developed to measure the surface area of locations where a coincidence of voxels from CD31 (endothelial cells/blood vessel) and GFAP (astrocyte) or desmin (pericyte) signals both occur. These areas of intersection represent where the astrocytes or pericytes have contact with the MVECs. Qualitatively an increase of astrocyte coverage was observed in the MPS IIIB mouse brains compared to those of the WT mice. This observation was quantitatively confirmed to be significant the capillaries of the cortex and to trend upward in all other measured vessels and regions. Additionally, since astrocytes are believed to induce the barrier-like quality in the endothelial cells through instructive cues that occur through their end feet contact points, we looked at how many points of contact the astrocytes made with the endothelial cells. We observed a significant increase in the number of astrocyte contact points made with blood vessels in capillaries from both the cortex and the thalamus in MPS IIIB compared to WT mice as well as a continued trending increase in both regions of the larger blood vessels. These findings provide evidence to support reports that astrocytes have roles in both maintaining the BBB in health and repairing the BBB when damage occurs.

To provide further support for our observations additional studies are required to determine if the observed increase in astrocyte-endothelial cell contact is indeed in reaction to BBB impairment. Mice used in this study were approximately 10 months old with disease manifestation well underway, in order adequately answer the questions regarding when the

astroglyosis and increased endothelial cell contact occur in relation to BBB permeability, a time course study of disease pathogenesis is required. Utilizing the tools described here the time points of when BBB leakage is observed can be correlated with when increased astrocyte-endothelial cell contact occurs, providing critical information into further understanding of this disease progression.

The effects of reported pericyte damage in MPS IIIB were analyzed by measuring the surface area of their coincidence with the blood vessel endothelial cells in the same manner as the astrocyte foot processes were. Interestingly no significant change was observed in these desmin positive pericytes in any region or blood vessel grouping between WT and disease. We find no convincing change therefore suggesting that swelling may not have a functional consequence. In fact when we measured to volume of these pericytes to analyze their swelling ourselves we saw no change. Several interpretations of this data are possible including that, contrary to literature, pericytes have a relatively minor role in BBB integrity. Additional interpretations include that pericytes are reported to be a heterogeneous cell type and no one marker can adequately access them at any one time. Therefore, while desmin positive pericytes had no observable change in blood vessel contact there could be changes to pericytes expressing PDGFRB, ASMA, or NG2 that simply need to be studied as well. A time course study, incorporating the analysis techniques developed here, as well as additional pericyte markers, is necessary in order to gain a better understanding of the pericyte population in this disease and as it relates to the BBB.

According to the literature endothelial cells in MPS IIIB are swollen but this is only explored in ultrastructure analysis and not in the context of the entire vessel<sup>31</sup>. Additionally we wanted to try and understand the changes in astrocytes that we identified. So we looked at the

endothelial cells and their TJs using CD31 as discussed earlier. When we looked at them we also saw an apparent disruption of the endothelial cells along their tight junctions suggesting there is tight junction damage as well. When the percent of intact MVEC along the blood vessels length was measured we observed a significant decrease in the amount of undamaged MVECs along the TJs in capillaries in MPS IIIB mice suggesting that the changes we observed in BBB structural components is in response to BBB damage.

From the observed results we created a visual model of the BBB in both WT and MPS IIIB (Fig. 21). In the WT model we have intact EC that equate to undamaged tight junctions, minimal astrocyte contact, and we saw desmin positive pericytes wrapping around the vessels. Then in MPS IIIB model we have the observed disrupted EC equaling damaged TJs, an increase of astrocyte contact area with the vessels for barrier support; as well as an increase in astrocyte contact points where they are instructing repair. Lastly no change in desmin positive pericyte contact area gave us no evidence of pericyte disruption contrary to what has been proposed in literature<sup>31</sup>.

The development of a detailed quantitative model of the BBB in both wild type mice and diseased states is a first of its kind. The novelty of 3D analysis provides precision to the study of vasculature interactions that has not been possible with 2D, and will reduce the margin of error that is typical in this type of analysis. Additionally, the information obtained from this characterization of the effect of disease on BBB integrity is invaluable in future drug treatment development plans including aiding in insight on disease pathology as well as developing strategies for drug delivery into the brain.

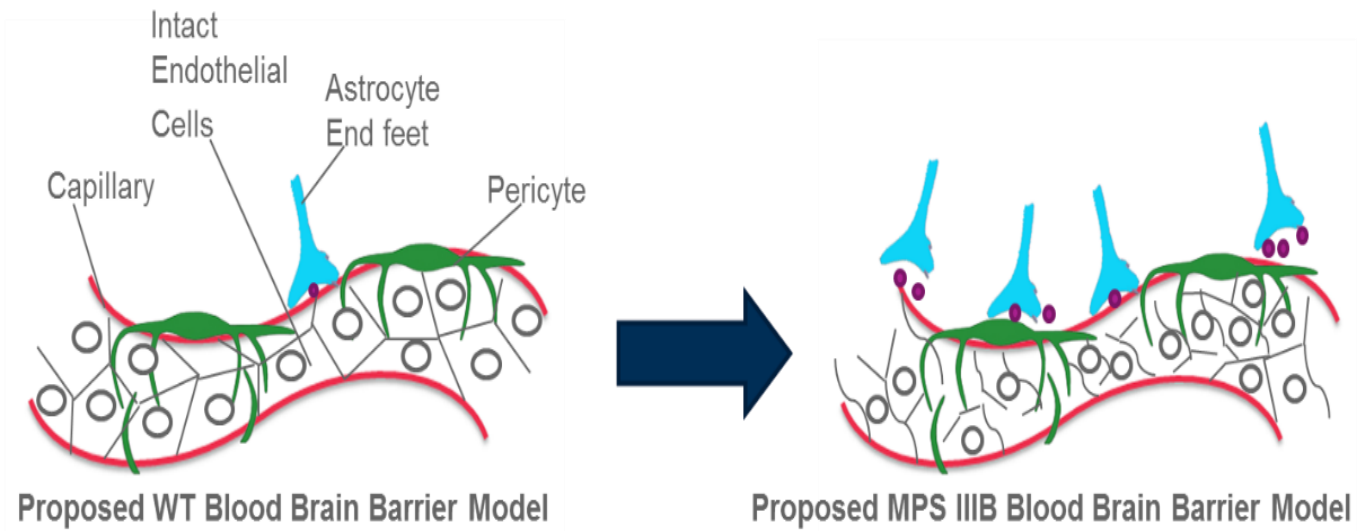


**Figure 21 Proposed Models of the BBB for WT and MPS IIIB** A) WT BBB model with intact endothelial cells, minimal astrocyte foot process contact, and pericytes wrapped around the blood vessel. B) MPS IIIB BBB Model with disrupted endothelial cell, increased astrocyte contact points and contact area and no change in pericyte coverage compared to the WT model.

## References

1. Ballabh P, Braun A, Nedergaard M. The blood-brain barrier: an overview: structure, regulation, and clinical implications. *Neurobiol Dis*. 2004;16(1):1-13. doi:10.1016/j.nbd.2003.12.016.
2. Weiss N, Miller F, Cazaubon S, Couraud P-O. The blood-brain barrier in brain homeostasis and neurological diseases. *Biochim Biophys Acta*. 2009;1788(4):842-857. doi:10.1016/j.bbamem.2008.10.022.
3. Hawkins BT, Davis TP. The Blood-Brain Barrier / Neurovascular Unit in Health and Disease. 2005;57(2):173-185. doi:10.1124/pr.57.2.4.173.
4. Zlokovic B V. The blood-brain barrier in health and chronic neurodegenerative disorders. *Neuron*. 2008;57(2):178-201. doi:10.1016/j.neuron.2008.01.003.
5. Pardridge WM. Blood – brain barrier delivery. 2007;12(January):54-61. doi:10.1016/j.drudis.2006.10.013.
6. Jones AR, Shusta E V. Blood-Brain Barrier Transport of Therapeutics via Receptor-Mediation. 2009;24(9):1759-1771. doi:10.1007/s11095-007-9379-0.Blood-Brain.
7. Xiao G, Gan L. Receptor-Mediated Endocytosis and Brain Delivery of Therapeutic Biologics. 2013;2013.
8. Winkler EA, Bell RD, Zlokovic B V. Central nervous system pericytes in health and disease. *Nat Neurosci*. 2011;14(11):1398-1405. doi:10.1038/nn.2946.
9. Alberts B, Johnson A, Lewis J et al. *Blood Vessels and Endothelial Cells*. Molecular . New York: Garland Science; 2002. <http://www.ncbi.nlm.nih.gov/books/NBK26848/>.
10. Bazzoni G, Dejana E, Farmacologiche R, Negri M. Endothelial Cell-to-Cell Junctions : Molecular Organization and Role in Vascular Homeostasis. 2004:869-901.
11. Abbott NJ. Blood-brain barrier structure and function and the challenges for CNS drug delivery. *J Inherit Metab Dis*. 2013;36(3):437-449. doi:10.1007/s10545-013-9608-0.
12. Luissint A-C, Artus C, Glacial F, Ganeshamoorthy K, Couraud P-O. Tight junctions at the blood brain barrier: physiological architecture and disease-associated dysregulation. *Fluids Barriers CNS*. 2012;9(1):23. doi:10.1186/2045-8118-9-23.
13. Wolburg H, Lippoldt A. Tight junctions of the blood – brain barrier : Development , composition and regulation. 2002;38:323-337.

14. Engelhardt B. Development of the blood-brain barrier. 2003;119-129. doi:10.1007/s00441-003-0751-z.
15. Moy AJ, Wiersma MP, Choi B. Optical histology: a method to visualize microvasculature in thick tissue sections of mouse brain. *PLoS One*. 2013;8(1):e53753. doi:10.1371/journal.pone.0053753.
16. Sofroniew M V, Vinters H V. Astrocytes: biology and pathology. *Acta Neuropathol*. 2010;119(1):7-35. doi:10.1007/s00401-009-0619-8.
17. Abbott NJ, Rönnbäck L, Hansson E. Astrocyte – endothelial interactions at the blood – brain barrier. 2006;7(January):41-53. doi:10.1038/nrn1824.
18. Abbott NJ. Astrocyte – endothelial interactions and blood – brain barrier permeability \*. 2002;629-638.
19. Willis CL, Nolan CC, Reith SN, et al. Focal Astrocyte Loss Is Followed by Microvascular Damage , With Subsequent Repair of the Blood-Brain Barrier in the Apparent Absence of Direct Astrocytic Contact. 2004;337(August 2003):325-337. doi:10.1002/glia.10333.
20. Zhou J, Kong H, Hua X, Xiao M, Ding J, Hu G. Altered blood-brain barrier integrity in adult aquaporin-4 knockout mice. *Neuroreport*. 2008;19(1):1-5. doi:10.1097/WNR.0b013e3282f2b4eb.
21. Rajkowska G, Hughes J, Stockmeier CA, Miguel-hidalgo JJ, Maciag D. Coverage of Blood Vessels by Astrocytic Endfeet. *Biol Psychiatry*. 2012;73(7):613-621. doi:10.1016/j.biopsych.2012.09.024.
22. Willis CL. Astrocytes. Milner R, ed. 2012;814:515-529. doi:10.1007/978-1-61779-452-0.
23. Avenue G. Endothelial/Pericyte Interactions. *J Am Heart Assoc*. 2005:512-523. doi:10.1161/01.RES.0000182903.16652.d7.
24. Nisancioglu MH, Wallgard E, Niaudet C, et al. Pericytes regulate the blood–brain barrier. 2010;(V):6-11. doi:10.1038/nature09522.
25. Bergers G, Song S. The role of pericytes in blood-vessel formation and maintenance. *Neuro Oncol*. 2005;7(4):452-464. doi:10.1215/S1152851705000232.
26. Omid Y, Barar J. Impacts of Blood-Brain Barrier in Drug Delivery and Targeting of Brain Tumors. 2012;2(1):5-22. doi:10.5681/bi.2012.002.
27. Sands MS. A Hitchhiker’s guide to the blood-brain barrier: in trans delivery of a therapeutic enzyme. *Mol Ther*. 2014;22(3):483-484. doi:10.1038/mt.2014.12.

28. Zlokovic B V. Neurodegeneration and the neurovascular unit. *Nat Med*. 2010;16(12):1370-1371. doi:10.1038/nm1210-1370.
29. Thal SC, Luh C, Schaible E-V, et al. Volatile anesthetics influence blood-brain barrier integrity by modulation of tight junction protein expression in traumatic brain injury. *PLoS One*. 2012;7(12):e50752. doi:10.1371/journal.pone.0050752.
30. Isasi E, Barbeito L, Olivera-Bravo S. Increased blood-brain barrier permeability and alterations in perivascular astrocytes and pericytes induced by intracisternal glutaric acid. *Fluids Barriers CNS*. 2014;11:15. doi:10.1186/2045-8118-11-15.
31. Garbuzova-Davis S, Louis MK, Haller EM, Derasari HM, Rawls AE, Sanberg PR. Blood-brain barrier impairment in an animal model of MPS III B. *PLoS One*. 2011;6(3):e16601. doi:10.1371/journal.pone.0016601.
32. Weber B, Guo X, Kleijer WJ, Kamp JJP Van De, Poorthuis BJHM, Hopwood JJ. Sanfilippo type B syndrome ( mucopolysaccharidosis III B ): allelic heterogeneity corresponds to the wide spectrum of clinical phenotypes. 1999;(May 1998):34-44.
33. Li HH, Yu W, Rozengurt N, et al. Mouse model of Sanfilippo syndrome type B produced by targeted disruption of the gene encoding  $\alpha$ -N-acetylglucosaminidase. 1999;96(25).
34. Heldermon CD, Hennig AK, Ohlemiller KK, et al. Development of Sensory , Motor and Behavioral Deficits in the Murine Model of Sanfilippo Syndrome Type B. 2007;63104(8). doi:10.1371/journal.pone.0000772.
35. Zafeiriou DI, Batzios SP. Brain and spinal MR imaging findings in mucopolysaccharidoses: a review. *AJNR Am J Neuroradiol*. 2013;34(1):5-13. doi:10.3174/ajnr.A2832.
36. Xue Q, Liu Y, Qi H, et al. A novel brain neurovascular unit model with neurons, astrocytes and microvascular endothelial cells of rat. *Int J Biol Sci*. 2013;9(2):174-189. doi:10.7150/ijbs.5115.
37. Shawahna R, Decleves X, Scherrmann J-M. Hurdles with using in vitro models to predict human blood-brain barrier drug permeability: a special focus on transporters and metabolizing enzymes. *Curr Drug Metab*. 2013;14:120-136. <http://www.ncbi.nlm.nih.gov/pubmed/23215812>.
38. Goldstein M, Watkins S. Immunohistochemistry. *Curr Protoc Mol Biol*. 2008;Chapter 14(January):Unit 14.6. doi:10.1002/0471142727.mb1406s81.
39. Lang E, Baier J, Kohler J. Epifluorescence , confocal and total internal reflection microscopy for single-molecule experiments : a quantitative. *J Microsc*. 2006;222(December 2005):118-123.

40. Meding S, Walch A. *Epi-Fluorescence Microscopy*.; 2013. doi:10.1007/978-1-62703-056-4.
41. Schermelleh L, Heintzmann R, Leonhardt H. A guide to super-resolution fluorescence microscopy. *J Cell Biol.* 2010;190(2):165-175. doi:10.1083/jcb.201002018.
42. Royal THE, Academy S, Sciences OF. Super-Resolved Fluorescence Microscopy. 2014;50005.
43. Cox G. Biological confocal microscopy. *Mater Today.* 2002;5(3):34-41. doi:10.1016/S1369-7021(02)05329-4.
44. Ragazzi M, Piana S, Longo C, et al. Fluorescence confocal microscopy for pathologists. *Mod Pathol.* 2013;27(3):1-12. doi:10.1038/modpathol.2013.158.
45. Saubaméa B, Cochois-Guégan V, Cisternino S, Scherrmann J-M. Heterogeneity in the rat brain vasculature revealed by quantitative confocal analysis of endothelial barrier antigen and P-glycoprotein expression. *J Cereb Blood Flow Metab.* 2012;32(1):81-92. doi:10.1038/jcbfm.2011.109.
46. Paul D, Cowan AE, Ge S, Pachter JS. Novel 3D analysis of Claudin-5 reveals significant endothelial heterogeneity among CNS microvessels. *Microvasc Res.* 2013;86:1-10. doi:10.1016/j.mvr.2012.12.001.
47. Janáček J, Cvetko E, Kubínová L, Travnik L, Eržen I. A novel method for evaluation of capillarity in human skeletal muscles from confocal 3D images. *Microvasc Res.* 2011;81(2):231-238. doi:10.1016/j.mvr.2010.11.012.
48. Macdonald JA, Murugesan N, Pachter JS. Endothelial Cell Heterogeneity of Blood-Brain Barrier Gene Expression Along the Cerebral Microvasculature. 2010;1474:1457-1474. doi:10.1002/jnr.22316.
49. Zudaire E, Gambardella L, Kurcz C, Vermeren S. A computational tool for quantitative analysis of vascular networks. *PLoS One.* 2011;6(11):e27385. doi:10.1371/journal.pone.0027385.
50. Biology D, Biology D, Regulation G, Sciences L, Dd D, Biology C. Evaluating performance in three-dimensional fluorescence. 2007;228(July):390-405.
51. Petzelbauer P, Halama T, Gro M. Endothelial Adherens Junctions. 2000:10-13.